UNIVERSITY OF CALIFORNIA
SANTA CRUZ

ESCAPE: ENERGY SCAVENGING COLLAR FOR ANIMAL PHYSIOLOGY AND ECOLOGY

A dissertation submitted in partial satisfaction of the
requirements for the degree of

DOCTOR OF PHILOSOPHY

in

COMPUTER ENGINEERING

by

Maxwell Lichtenstein

December 2020

The Dissertation of Maxwell Lichtenstein
is approved:

Gabriel Elkaim, Chair

Katia Obraczka

Chris Wilmers

Quentin Williams
Vice Provost and Dean of Graduate Studies

Table of Contents

List of Figures

List of Tables

Abstract

ESCAPE: Energy Scavenging Collar for Animal Physiology and Ecology

by

Maxwell Lichtenstein

Animal tracking tags are a useful tool in the study of wild animals and ecological systems, but the process of tagging an animal is costly and often traumatic for the animal. For many types of tags, the lifetime of the tag is determined by battery life. The Energy Scavenging Collar for Animal Physiology and Ecology (ESCAPE) project investigates several methods for reducing overall power consumption in wildlife tracking tags. This work develops and tests several algorithms for reducing GPS uptime in these tags, using Extended Kalman Filters to guide uncertainty-suppression GPS scheduling. These algorithms use less costly sensors such as accelerometers, magnetometers, and gyrometers to augment GPS in estimating locations during tracking. We implement and test these algorithms in tests on human subjects. This work also includes analysis of several proposed techniques for scavenging energy in the field, such as harvesting excess kinetic and thermal energy from the animal. Our analyses provide upper bounds on expected power returns from these strategies, providing useful metrics for determining whether such strategies are viable regions of the tag design space. The findings of the ESCAPE project contribute to future tag research and development by highlighting strategies with potential for improving tag lifetimes, and discouraging other strategies.

To my parents and brother, whose boundless support and love kept me afloat; to Gabe, who gamely put up with me for so many years; to the various members of the Autonomous Systems Lab, with whom sharing creative space has been an unparalleled joy; and to Max D, whose collegiality and camaraderie is an education unto itself.

Acknowledgments

My greatest misunderstanding when undertaking this project was in underestimating, vastly underestimating, the amount of help it would require. Where I have succeeded, I have done so with the selfless support of others. Where I have failed, I have done so by neglecting to seek such support. An exhaustive enumeration of thanks would be too long to fit here, or even in my recollection, so I apologize to those I miss. Nonetheless, I shall try.

My advisor, Gabe Elkaim, has given me freedom to explore a project of unusual breadth. Though the territory has been dauntingly large, I know of no other advisor who could support me through its many terrains. This exploration would be meaningless without the perspective and wisdom of my committee members. Chris Wilmers has kept me grounded, reminding me that the things that we engineers engineer are meant for the real world. Katia Obraczka has kept me lucid about my own field and what I can bring to it. Though Terrie Williams and Ren Curry are not official members of my committee, their insights have been nonetheless invaluable. And I also thank Leila Parsa, whose last-minute assistance rescued me from a difficult situation.

Countless peers have contributed in myriad ways to this project, from entertaining my wild ideas, wrangling whiteboard calculations, proofreading drafts, and showing me my mistakes. Thanks to labmates John Ash, Bryant Mairs, Dmitri Rivkin, Sharon Rabinovich, Pavlo Vlastos, Joran Liss, Danny Eliahu, Chris Seruge, Vijay Muthukumaran, David Goodman, and many others whose omission on this list is lamentable. Special thanks to Yiwei Wang and Caleb Bryce, whose work has been foundational to this project, and who showed me what ecologists do. Also, thanks to the interns who contributed directly to this project, including Molly Graham, Oliver Rene, Josh Gier, and Carl Lindquist. And of course, many

many thanks to Max Dunne, whose work is the giant on whose shoulders my own research stands.

A round of thanks to my family and friends. While most people on this list have lightened the load, like an uptime-reducing sensor scheduling algorithm, you have given me energy along the way, like a solar panel or kinetic harvester. Thanks to all my friends, but especially Barrett Anderson, Samantha Egle, Blake Ritchen, Cary Shapiro, and Michelle Hua. You're a good bunch.

I should also thank the National Science Foundation, who provided funding for the ESCAPE project. I hope you find the money well spent.

I also must thank the institution that has given me this opportunity, the University of California Santa Cruz, and also Emily Gregg, without whom that institution would have been entirely un-navigable. Thanks to Megan Paciaroni, who motivated me to pursue a graduate education, and to Jacob Rosen, who opened the door to this particular school.

And finally, thanks to the many professors who have taught me, and another round of thanks to the professors who hired me to teach. Perhaps most of all, thanks to my many students, for helping you has been an invaluable source of joy and purpose throughout this journey.

Chapter 1

Introduction

1.1 Problem Statement

Animal tracking tags are a useful tool in the study of wild animals and ecological systems, but the process of tagging an animal is costly and often traumatic for the animal. For many types of tags, the lifetime of the tag is determined by battery life. Modern tags carry a suite of electronics to monitor sensors, record results, and communicate wirelessly with ground stations. These activities, though highly useful, consume energy and eventually deplete the tag's batteries. This either ends the experiment, or necessitates a costly re-tagging process.

In general, higher-quality data requires more energy. Sensors such as Global Positioning System receivers (GPS) and accelerometry draw more power as their sample rates increase. Furthermore, the data they acquire must be stored or transmitted to a base station, which also draws power. This produces a tradeoff for the designer of an ecological experiment: The lifetime of the project can be increased by sacrificing quality, or vice-versa. But, if techniques can be found which decrease the power consumption of the tag without sacrifice to the quality of the final data, the tradeoff would be eased and the utility of tracking tags would

be increased.

A variety of methods have been proposed or explored for improving tag lifetimes. Battery life can be enhanced by supplementing the battery with energy scavenged from the environment or the animal itself. Some of the scavenging methods that have been proposed or explored are solar power, kinetic energy from the animal's motion, and thermal energy from the animal's body heat. On the other side of the energy budget, battery life can be improved by reducing the power spent by the collar. This can be accomplished in hardware by leveraging low-power electronic technology, or in software by improving the power policy of the tag to conduct its tasks more efficiently.

This work, the Energy Scavenging Collar for Animal Physiology and Ecology (ESCAPE) is an NSF-funded project that investigates these methods to reduce the overall power usage of wildlife tracking tags. In this work, we design and test a tag that synthesizes these technologies to provide insight into how they can be used, and lay groundwork to improve the state-of-the-art in tag design. This project is a successor project to the ANIMA project, another NSF-funded project with similar goals (Dunne 2014).

The ESCAPE project explores two general methods for improving tag design: Energy scavenging and sensor scheduling algorithms.

1.1.1 Background

Wildlife Tags

Systematically tracking the motion of wild animals is at least as old as 1710, when unnamed naturalists attached a metal ring to a heron, determining that it migrated from Turkey to Germany (Lincoln 1921). The technique of attaching physical "tags" to animals is a relatively low-cost system for monitoring wildlife

movement, and has been a standard approach ever since.

Modern tags can carry electronics. As R.E Kenward recounts, the development of the transistor spurred development of small radio-wave transmission devices in the early 1960s(Kenward 2001) . Early experiments with the technology included a 1959 attempt to implant heart-rate sensors in chipmunks, and a 1960 test of a heart- and wing-beat sensor mounted on mallards. These experiments involved encoding sensor results as frequency-modulated signals, which researchers listened to using a radio receiver. These early forays into radio-transmission technology were used to observe the physiology of captive animals, but limited battery life prohibited monitoring animals traveling in the wild.

During the 1960s, several researchers innovated the use of pulsed radio signals (Cochran and Lord 1963), which extended the lifetime of the transmitter, and allowed human ears to detect faint signals. The combination of longer lifetimes and longer detection ranges enabled the tracking of animals over longer periods of time, and over wider distances. Localization could now be performed using directional antennas and triangulation, and sensor readings could be transmitted along with the tracking signal ((Kenward 2001), (Schmutz and White 1990).

In 1980s, the US Air Force made its Global Positioning System available for public use. This triggered the development of a wave of new animal tracking devices which could perform localization with greater accuracy and automation (Rodgers 2001), though at cost and with a new set of design considerations. In general, GPS systems require more power than pulsed radio transmissions, and occupy a greater volume than a radio transmitter, limiting the use of GPS technology in smaller animals.

A tag designer must consider how to deliver data from the tag to the researcher. One option is to record data on the tag, using an SD card or chip memory, but

this “store-on-board” method only postpones the transfer. A radio transmitter may transmit bursts of data at specified intervals. It might also be paired with a receiver, and transmit a payload in response to a command signal. A second option is a drop-off tag, which does not transmit logged data at all, but instead transmits enough information to allow a researcher to retrieve the tag once battery reserves fall below some threshold. A tag may automatically fall off the animal, or remain on the animal to allow re-capture. Either strategy requires some sort of transmission capability.

These techniques are all useful, but each new feature consumes more energy, forcing ecologists to make strategic tradeoffs between the lifetime of a study and the depth of data it can collect. New technologies that save energy can mitigate these tradeoffs, and energy scavenging technologies carry the tantalizing possiblity of removing the tradeoff altogether.

Energy Scavenging

Early spacecraft research forms the origin of much of the analysis and many of the technical principles that inform the design of hermetic, energy-scavenging devices in other fields. C.M. MacKenzie, in an early example, lays out the basic techniques for modeling and budgeting power use on a solar-powered orbital satellite (Mac Kenzie 1967) . The intensity of solar radiation near the earth is quite high, so solar power is a widespread scavenging technique. For many spacecraft, this source is sufficiently powerful and consistent to enable energy neutrality. On the surface of the earth, however, this resource is only available during the day, and during suitable weather.

For systems that are mounted on a living animal, the animal itself is a potential source of free energy. Animals, by their nature, collect chemical energy in the form

of food and convert it to various other forms, including kinetic energy for motion and thermal energy to maintain physiological functions. Animals generally use energy with imperfect efficiency. They exert more force than they require to move. Their internal physiological processes produce excess heat, which must be radiated out into their cooler environment. This energy is lost to the animal, but some of it could theoretically be captured to do useful work.

When designing scavengers, it is essential to also consider the impact of the scavenger on the animal's daily life. An animal would experience a kinetic scavenger as though it were actively resisting or modifying its movement, and would likely hear some audible feedback. Solar panels are reflective, which can produce visual alerts to predators or prey (Marks and Marks 1987), (Burger Jr et al. 1991). Any type of scavenging device would add weight to the final design, which could tax the animal's strength and endurance.

Thus, in deciding whether to add new scavenging technology to a collar design, we must have a reasonable model of the tradeoffs that technology introduces. While each of these technologies has been studied in other domains, less research considers the applicability of these techniques to animal tracking, and we have yet to find a source that provides explicit descriptions of the capabilities and limitations of this technology in a form that is readily accessible to ecologists.

Adaptive Sampling

Scavenged energy is one of two components in the net power consumption of a hermetic device. Another promising avenue for extending the battery life of a hermetic device is to reduce power consumption. Since GPS measurements are far more expensive than accelerometry measurements (Dunne 2014), our strategies aim to reduce GPS measurement frequency by leveraging information from

accelerometry.

One simple strategy is a mode-based sampling policy, similar to the one deployed in A. M. Wilson's cheetah collars(Wilson et al. 2013). In this strategy, the target animal's behavior is classified into distinct modes, which can be identified using accelerometry in real-time. Y. Wang provides an algorithm for classifying mountain lion behavior into three categories of ground movement, which could be utilized to enact this strategy(Wang et al. 2015).

In this work, we explore several uncertainty-suppression strategies. In these strategies, sensor data is used to maintain some estimate of the tag's position, and also some measure of the uncertainty in that estimate. The uncertainty grows in the time between successful GPS measurements, but crucially, the rate of uncertainty growth is dependent on accelerometry data. Once this uncertainty reaches some threshold, a GPS measurement is triggered, and the uncertainty is reduced. We explore several uncertainty suppression algorithms with varying complexity and sensor sets, as described in Section 4, as well as our prior work(Lichtenstein and Elkaim 2019),(Lichtenstein and Elkaim 2020).

1.1.2 Related Work

Modern wildlife tags can be considered as nodes in a wireless sensor network ("WSNs"). This is a broad class of devices, including applications in military technology, agriculture, geology, oceanography, smart homes, and personal communication. Research on WSNs has been active since at least the early 2000s, and is continuously spurred by new advances in battery technology and wireless transmission ((Tan, Wilson, and Lowe 2008), (Wan, Tan, and Yuen 2011)).

These devices are widely varied, with diverse demands on size, reliability, communication bandwidth, connectivity, and longevity, but all face the same core chal-

lenge of balancing functionality and longevity across the fulcrum of their energy supply. We draw heavily from the literature on WSNs, particularly in the areas of energy scavenging, size minimization, and adaptive transmission and sampling.

Another related field is wearable technology. "Wearables" are a class of device meant to measure or interact with the human to which the device is attached. These are increasingly common as medical sensors (Romero, Warrington, and Neuman 2009), and also as consumer electronics. Wearable technology faces almost the same set of design constraints as wildlife tagging: They must be small, lightweight, and generally record similar types of information such as accelerometery and location. The most pertinent difference is that wearables benefit from the cooperation of their animal, who can recharge depleted batteries, protect fragile electronics, and replace malfunctioning equipment. Nonetheless, Wearable research provides useful insight into the design of animal-mounted sensors, and experiments in this domain are easier to conduct.

Research into software design in Personal Communication Services ("PCS") devices is also relevant to the adaptive sampling portion of this work. These devices, which include mobile phones, are similarly tasked with balancing high-power location tracking against battery life. This field is especially rich in research into adaptive sampling and transmission. The ubiquity of PCS devices gives PCS research a vast amount of data, and allows experimentation with a wide variety of novel techniques.

Finally, our work is guided by other research in ultra-low-power animal tagging technology. Understandably, most ecologists are not preoccupied with the technical details of tag design, so detailed work on novel power design in wildlife tags is sparse, but where it exists it is immensely valuable. A few tag design projects stand out with promising results in low-power electronics, energy scav-

enging, and adaptive power policy: ZebraNet (Juang et al. 2002), (Zhang et al. 2004), wildCENSE (Jain et al. 2008), AMBLoRa (Antoine-Santoni et al. 2018), Wilson's cheetah tracking collar (Wilson et al. 2013), CARNIVORE (Rutishauser et al. 2011), Shafer's avian-mounted kinetic harvester (Shafer 2013), Camazotz (Jurdak et al. 2013a), (Sommer et al. 2016), and ESCAPE's predecessor project, ANIMA (Dunne 2014).

Chapter 2

Tag Design

2.1 The State of the Art in Tag Design

Before examining potential improvements to the state of the art in tag design, we must first examine the current state of the art. In particular, we are interested in the power budgets of current tags, and in commonalities and distinctions in their designs.

The space of tag designs is large, reflecting the variety in research goals and animal physiology. To narrow the scope of our investigation, we focus on designs with well-documented power budgets that utilize GPS, accelerometry, and long-term data storage, and that are built for larger terrestrial animals.

The CARNIVORE tag (Rutishauser et al. 2011) is particularly useful because it documents the collar used to gather the 36M dataset in (Wang et al. 2015), which informs our scavenging and adaptive sampling designs. The ANIMA tag (Dunne 2014) contains a very thorough comparison of component choices for accelerometers, magnetometers, and GPS, tested in an outdoor wooded environment. (Jurdak et al. 2010) and the Camazotz system in presented in (Jurdak et al. 2013a) additionally provide detailed power budgets, and the latter includes

a solar scavenger.

A few more designs did not present detailed power budgets, but do provide detailed information about various technical design elements. The ZebraNet system (Juang et al. 2002, Zhang et al. 2004) explores a variety of low-level power topologies for synthesizing solar scavenged energy with high-current GPS sensors. (Wilson et al. 2013) also provides a detailed account of their design choices for their cheetah tracking collars.

2.1.1 Power Consumption

We begin our exploration of existing tag designs with an examination of their power budgets.

Figure 2.1 compares power budgets from these projects. We observe some commonalities in each design. First, the GPS system dominates nearly every budget, even in projects that strongly duty-cycle their GPS modules. Radio modules and data logging also consume large shares of power budgets, with some trade-off between them. Microcontrollers are generally moderate in their power use, as long as low-power models are selected, and their low-energy modes utilized. Accelerometry and other on-board sensing systems merely sip at batteries.

By far, the most efficient design is Camazotz, from (Jurdak et al. 2013b). This design achieves its low power budget primarily with a very aggressive power policy, using a wide range of low-power sensors to carefully ration expensive measurements. We discuss these strategies thoroughly in Section 4

2.1.2 Electronic Design

Though early tags used different topologies, nearly all modern tags use a standard embedded controller design as their top-level structure. In this topology, a

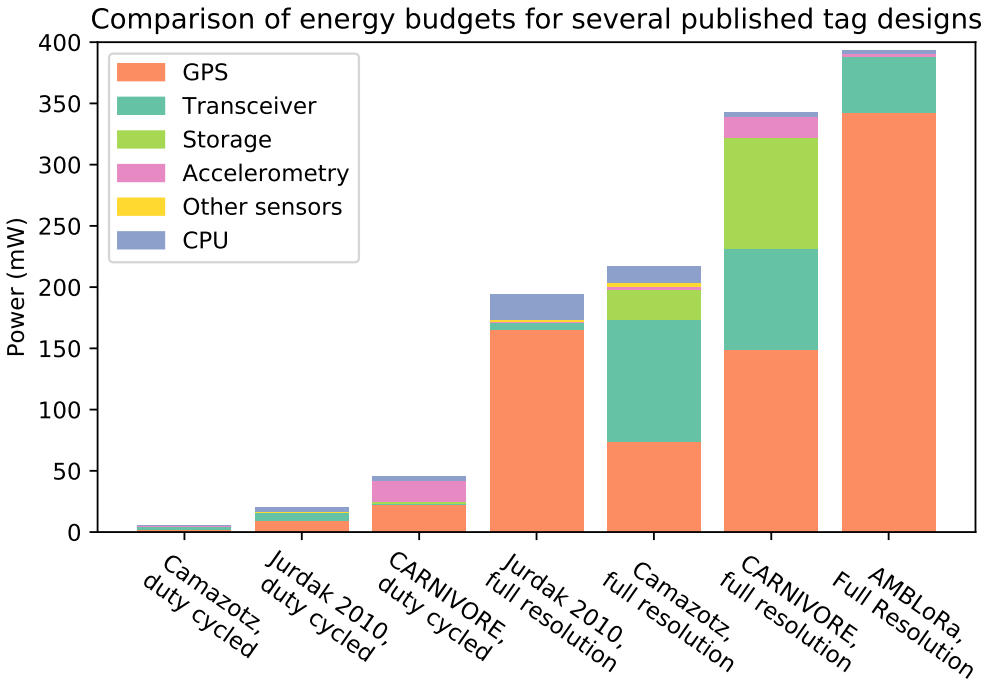

Figure 2.1: Comparison of energy budgets for several published tags. CARNIVORE's duty-cycled GPS power was recorded at a 20 minute period. In this figure, the value was extrapolated to match the 5 minute period used in (Wang et al. 2015). Note that AMBLoRa and and Jurdak 2010 do not use data storage.

Tag	Processor	GPS	IMU	battery
AMBLORA	Microchip PIC24FJ128GA310	Origin GPS ORG1208	Analog Devices Inc ADXL345 (Accel only)	unspecified
CARNIVORE	Texas Instruments MSP430	Lassen iQ	MMA7260Q (Accel only)	2 Li AA-cell
Camazotz	Texas Instruments MSP430 (as part of Texas Instruments CC430F5137)	u-blox MAX-6	STMicroelectronics LSM303 3 (Accel and Mag)	Li-Ion
Jurdak 2010	Atmel-1281 MCU	u-blox MAX-6	not included	unspecified

Table 2.1: Hardware design overview of selected tags.

central processing unit is responsible for controlling the other components of the collar, and for moving data between them. This design is ubiquitous because it simplifies the design process, and because it provides the designer flexibility after the hardware is constructed by reprogramming the controller.

We begin by considering the basic electronic design of several peer tags. Table XXX compares the processor, GPS unit, IMU sensors, and battery type for several tags.

Several of these tags carried additional peripherals. Camazotz also carried a microphone and a pressure sensor. The Camazotz tag carried a radio transmitter with an integrated microcontroller, and Jurdak 2010 and AMBLORA carried peripheral radio transmitters as well.

One notable commonality is that each of these tags utilize a microcontroller that is marketed as a low-power device. This partially explains the low contribution of the CPU to the various power budgets described in Figure 2.1, and further suggests that there are little additional gains to be made by optimizing CPU choice further.

Chapter 3

Energy Scavenging in Animal Tags

A wide variety of sources of useable energy are available in the environments that animals navigate. T. Starner suggests that human wearables could harness body heat, air flow from exhalation, force from chest expansion and pulsing blood pressure, inertial motion from arms and fingers, and striking motion from footfalls (Starner 1996). Various other blue-sky surveys add ambient light, ambient radio emissions, and acoustic vibration to the mix (Romero, Warrington, and Neuman 2009; Sravanthi Chalasani and Conrad 2008).

We first discuss some of the less common proposals.

Radio frequency (RF) scavenging has the advantage of being simple to implement, requiring only an antenna and a rectifier, which is well-suited to the geometry of a collar. (Lu et al. 2015) provides an exhaustive overview of techniques. However, typical results for ambient RF harvesting, using portably-sized antennas, in urban environments, produce power in the microwatt range (Piñuela, Mitcheson, and Lucyszyn 2013). Wildlife environments are generally more distant from RF transmitters, and so would almost certainly produce less power.

(Shafer et al. 2015) proposes a system to capture energy from changes in ambient pressure. This could be suitable for deep-diving marine animals, but not for terrestrial animals.

It is also possible to scavenge muscle motion by directly using muscle force to deform a flexible transducer. For example, (Starner 1996) shows that piezoelectric ribbons can be used to gather energy from the stretching and relaxing of an elastic band, and (Churchill et al. 2003) bonds a piezoelectric strip to a flexing beam to power a transmitter. Such a strip could easily be fitted into the band of a collar to capture any deformations that occur. However, near the 1 Hz frequency that characterizes puma motion, these deformations are unlikely to yield significant power.

(MacVittie et al. 2013) and (Halámková et al. 2012) use implantable biofuel cells to harvest energy directly from glucose in the bloodstream of snails and lobsters. While this technology presents some interesting avenues for research, we find it inappropriate for the ESCAPE project for a variety of reasons.

After considering the above, we found three categories of harvester to merit further analysis and experimentation: Solar scavenging, thermal scavenging, and inertial scavenging.

3.1 Scavenging Power Electronics

In evaluating the utility of a harvester, a designer should not neglect considering the circuitry that captures the power. Most research tests harvesters independently of a power load (such as electronic sensors or battery charging stages), but this can lead to signficiant overestimation of a harvester's power generating ability for reasons discussed below.

Integrating a scavenger in a circuit is non-trivial. One problem is that each

scavenger produces an output voltage that is considerably less than the voltage required to charge a lithium-based battery or power the onboard electronics of a tracking tag. One option is a power conditioning circuit, such as a DC-DC step-up converter ("boost converter") or a charge pump. These systems trade current for voltage, at the cost of less than 100% efficiency. Another option is to connect several scavengers in series, so each contributes to an overall supply voltage that could be sufficent to drive the electronics payload. These two methods can be deployed in tandem, as (Carreon-Bautista et al. 2014) shows in a design that reconfigured the circuit topology of the scavengers during operation for optimized efficiency.

A further difficulty in the domain of animal-mounted scavenging is the inconsistency of each scavenger's output. TEGs produce more energy at night, solar panels produce a trickle of energy during the day with spikes as the animal ventures into the sun, and kinetic scavengers produce bursts when the animal is mobile. No single source can be used to directly power the tag, so some system is required to store the extra energy each scavenger produces.

The design is further complicated if we wish to optimize the power output of each device. Each harvester type has a characteristic I-V curve, describing the current that the harvester will output if the voltage across its terminals is held constant. For a TEG under a given temperature differential, this curve is linear. For solar cells under constant illumination, this curve is a steady plateau with a relatively sharp drop-off (often modeled as an exponential curve, as in Sera, Teodorescu, and Rodriguez 2007). The I-V curves of thermopiles and rectified kinetic generators are often modeled as straight lines with negative slopes, corresponding to a constant voltage source and a constant resistance in series. In the context of a harvesting circuit with power conditioning, this curve should be

multiplied by the efficiency of the conditioning circuit. Assuming the power conditioning circuit consists of an ideal boost converter charging a battery, the $I(v)$ curve should be multiplied by a factor of $v/V_{battery}$.

The power scavenged by any device is, at most, the product IV, which means that there is a particular point on the IV curve at which maxmimum power is produced, which can be identified numerically from a measured IV curve, or analytically given a mathematical model of the curve. This is the "maximum power point," or MPPT. An ideal power harvesting circuit should constrain the generator to the vicinity of that point, either by controlling the current drawn from the device, or by controlling the voltage of the load. This is called "load-matching."

If an energy harvester operates under consistent conditions, such as photovoltaics on a spacecraft, load-matching can be designed in the hardware. Otherwise, the MPPT changes with illumination, ambient temperature, or frame acceleration, and some sort of feedback-control scheme is required to "track" the maximum power point.

3.2 Evaluating Scavenging Devices

The size and weight of tags are generally bounded by the physiology of the animal and the ethical obligations of researchers. Therefore, any harvester hardware takes some resource that could be expended on extra batteries. In order to be worth its weight and volume, an energy scavenging device must generate more energy than it displaces. More formally,

$$\overline{P_{scavenger}} \cdot T_{expected} > m_{scavenger} \cdot e_{primary}$$

$$\overline{P_{scavenger}} \cdot T_{expected} > v_{scavenger} \cdot u_{primary}$$

where $\overline{P}$ is the time-averaged power that the scavenger generates, T is the lifetime of the tag, m is the mass of the scavenger, e is the specific energy of the primary battery (energy per unit mass), v is the volume of the scavenger, and u us the energy density of the primary battery (energy per unit volume). [1]

3.3 Kinetic Scavenging

Kinetic energy scavengers work by harvesting some of the energy that the animal expends to move its body. As the animal moves, it exerts a force on the frame (or "stator") of the device, thereby adding energy to it. The kinetic generator then captures some of this energy. It is necessary that the generator contain a proof mass that can move relative to the stator, but which is coupled to the frame with some sort of electro-mechanical transducer. This coupling allows the stator to do negative mechanical work on the proof mass and capture some of that work in the form of electrical energy.

Kinetic power is not necessarily useful in all domains, however. As the laws of mechanics dictate, the power that can be harvested from external motion varies strongly with the speed, frequency, angle, and length of the motion. Human wrists move frequently, often in long strokes, often rotating over a wide angle. As we and others show, this is a desirable set of conditions for the designer of a kinetic scavenger. Many other devices must scavenge from slight, regular motion. These devices require a different design approach and have a lower ceiling on the amount

[1] An observer might note that these equations imply that an energy-positive scavenger has greater energy density and specific energy than the primary battery, so the scavenger should be scaled up and the primary battery removed entirely. This is unfeasible for most scavenging designs, though, whose forms are generally constrained by the principles of their operation. Solar panels, for example, should occupy only the outer surface of the tag. The lone exceptions are inertial harvesters, which we discuss in greater detail below.

of power that even an ideal design can produce. This is a particularly difficult barrier for collars mounted on the necks of terrestrial quadrupeds, which move far less than their extremities.

Most research into animal-mounted kinetic energy scavenging has been directed at humans. The advent of personal timepieces prompted the development of self-winding watches (Watkins 2013), and the medical utility of pacemakers and long-term physiological sensors for humans have driven the research in this arena (Romero, Warrington, and Neuman 2009).

The first credibly recorded self-winding watch was constructed in 1776 or 1777, using a sliding weight with a ratchet to wind a spring. Even this early prototype could gather a day's worth of power in the course of 15 minutes in the pocket of a human walking at an ordinary pace, demonstrating the potential of this type of energy scavenging. Most scavenging watches do not convert kinetic energy into electricity, but rather store the energy mechanically in a mainspring. There are a few exceptions, such as the Sieko Kinetic, the Sieko AGS, and the ETA SA (Romero, Warrington, and Neuman 2009).

Currently, a new wave of devices use motion to power various other types of devices in various locations on or in the human body. Consumer electronics attached to clothing ("wearables") are becoming increasingly commonplace, as are devices embedded in objects such as tennis rackets and skis. Novel research is exploring devices that can be embedded in the human body to provide health monitoring and pacemaking. Still other research is exploring devices that can be attached to vehicles and industrial machines, with the hope of making fully wireless and self-sustaining sensors that can be attached wherever they are needed

A few researchers have attempted kinetic scavengers for wildlife tagging. (MacCurdy et al. 2008) proposes a piezoelectric scavenger to mount on hawkmoths and

barnswallows. (Aktakka, Kim, and Najafi 2011) constructed a spiral-beam piezoelectric generator, meant for mounting on the back of a Green June Beetle. The device was tested on a vibrating stage mimicking the beetle's flight, where it produced 45 uW. (Snowdon et al. 2018) tested a piezoelectric cantilever on a falcon in flight, generating a maximum of approximately 3uW. (Shafer 2013) gives a very thorough account of an experiment to harvest energy from rock pigeons during flight, yielding 0.1-0.3 mW. As far as we know, no kinetic scavenger has been mounted on a terrestrial non-human animal, though (Wu et al. 2014) proposes a design which is targeted at large terrestrial animals, and (Wijesundara et al. 2016) prototyped a design for elephants. Wu's design takes the unusual approach of dangling a pendulum below the collar, and using mechanical rectification rather than electrical rectification to produce a direct current.

3.3.1 Categorizing Kinetic Harvesters

Kinetic harvesters can be categorized in many ways [2]. We focus on three main categories: We first consider the mechanism by which kinetic energy is transduced into electrical energy. Three practical methods for this are electromagnetic induction, electrostatic damping, and piezoelectric damping. A second categorization distinguishes between scavenger geometries. Scavengers are typically either linear, rotational, or a hybrid obtained by mounting linear mechanisms on rotating platforms. Finally, we consider whether the scavenger is resonant or non-resonant. Resonant scavengers are optimized to harvest energy from motion with a specific, predictable frequency, whereas non-resonant scavengers are built to capture energy from less-predictable motion.

In the analyses below, we always assume that the motion of the stator is unaf-

[2] See (Cepnik, Lausecker, and Wallrabe 2013) for a thorough categorization analysis

fected by the activity of the harvester. In other words, we assume the mechanical impedance of the force driving the stator is effectively zero. In the domain of animal tags, this assumption should be valid, since tags are designed to be unobtrusive to the animal. Relaxing this assumption would not only complicate the analysis, but also violate an ESCAPE design constraint.

Also note that the phrase ”kinetic scavenger" is a bit broader than the types of scavenger discussed here, including force- and impact-based scavengers. This chapter is focused on the subcategory of kinetic scavengers which rely on moving a proof mass, commonly called "inertial" scavengers.

Harvester geometry

Both rotational and linear accelerations in the stator can conceivably be harvested. In practice, mechanical design considerations generally force harvesters to select one or the other, and additionally to select an orientation for the harvester.

In a linear harvester, the motion of the proof mass is constrained to a line, or else has a very small range of motion which is approximately linear. This is generally accomplished with a hollow tube (Halim and Park 2014) or a cantilever. The primary advantage of the linear harvester is design simplicity, allowing a generator with few moving parts. Simple cantilevers can be incorporated in MEMS designs, as in (Kulah and Najafi 2004) or (Mitcheson et al. 2007).

In a rotational harvester, the proof mass rotates on an axis, scavenging rotational stator motion. In this case, inertial scavenging is proportional not the to the proof mass's total mass, but rather its moment-of-inertia. If the proof mass is shaped as a pendulum (usually a half-disk), the rotational harvester gains two advantages. Firstly, it can harvest some linear motion, as long as the linear motion has a component that is perpendicular to the pendulum's axis and current

angle. And secondly, if the axis is not vertical, then gravity acts on the pendulum as well.

In addition, there are various mechanisms for achieving hybrid geometries. Hybrid geometries may be useful if the desired geometry of the coupling mechanism does not match the type of motion. For example, (Pillatsch, Yeatman, and Holmes 2012), rolls a large iron cylinder over a series of piezoelectric cantilevers, plucking each one in turn, converting the oscillating tilt of the roller's track into approximately linear vibrations on the cantilevers. Hybrid geometries are also useful when the absolute orientation of the harvester is variable, while rotational oscillations about that orientation are regular. This is often the case in animals, which move with a regular stride, but often are moving on an incline. One approach here is to mount linear oscillators on a rotational stage, as in (Pillatsch, Yeatman, and Holmes 2014). Another is to mount magnets in meshes which act as 3-dimensional springs, several of which are reported in (Cepnik, Lausecker, and Wallrabe 2013)

More exotic geometries attempt to scavenge from motion along or about multiple axes. The literature includes spherical generators (Bowers and Arnold 2008), planar generators (Yang, Wang, and Zhang 2011), (Li et al. 2013), and fluid-based generators (Choi et al. 2011), to name a few. While these geometries may be useful, we find that they suffer from at least one of the following drawbacks: a low power density, high fabrication difficulty, or a large minimum volume.

Resonant vs Non-resonant Harvesters

In many domains, the ambient vibrations have a regular spectrum that is known beforehand. In this case, a kinetic scavenger could be deployed that is constructed and tuned to resonate at the peak frequency of the ambient vibra-

tions. This is a resonant harvester. Resonant harvesters are generally modeled as damped simple harmonic oscillators, where the damping force is a combination of mechanical friction and the coupling to the harvesting circuit. The dynamics of the simple harmonic oscillator are well understood, allowing relatively simple analytic estimates of key properties of this generator.

However, in other domains, the ambient vibrations may not be particularly regular. The ambient vibrations may be consistently periodic, but the frequency of the motion is variable, such as the engine of a car. In this case, the resonant frequency of the harvester can be tuned to match the motion. This can be done electrically by modifying the electrical load on the capture circuit (Roundy and Zhang 2005).

In some domains, regular oscillations are present, but at a low frequency. This is the case with stride motions for humans and pumas, whose stride frequencies are typically in the neighborhood of 1 Hz. These motions can be captured by resonant harvesters using mechanical frequency up-conversion, where a large, low-frequency proof mass strikes or plucks a smaller, high-frequency proof mass. The resulting "ringing" vibrations can the be harvested, usually at a higher efficiency. Some examples are (Pillatsch, Yeatman, and Holmes 2012), (Pillatsch, Yeatman, and Holmes 2014), (Sari, Balkan, and Külah 2010), and (Halim and Park 2014).

Coupling Mechanisms

One coupling method is electromagnetic induction. In this method, the proof mass carries a magnet, or is mechanically linked to a magnet. The stator carries an inductor that is near or along the magnet's path of motion, so that the magnet's motion produces a changing magnetic field through the inductor. By Faraday's law, a changing magnetic field through an inductor produces an electromagnetic

force across the wire of the inductor, which can be captured. Electromagnetic induction has several advantages, but perhaps the most pertinent is that the strength of modern magnets allow electromagnetic harvesters to achieve a high specific power, with relatively high output voltages.

A second method is piezoelectric activation. Piezoelectricity is a property of some crystalline materials that causes a voltage difference across the material when mechanical stress is applied. Piezoelectric crystals can form strike plates, harvesting energy from direct impacts. A more common form factor is the cantilever, where the voltage produced is approximately proportional to the bend of the beam. Piezoelectric harvesters have the advantage of mechanical simplicity. The only moving part in most piezoelectic designs is the cantilever, to which the proof mass is directly attached. The cantilever is very nearly a linear system, and can be tuned relatively easily, making these a common choice for resonant harvesters at higher frequencies.

The final coupling mechanism is electrostatic coupling. In this method, two conductors are placed near each other to produce a variable capacitor. A bias voltage is established across this capacitor. One or both conductors are allowed to move, and as the distance between the two changes, so too does the capacitance between them. This produces a change in the voltage across the plates, which can be harvested. This is essentially the same setup that microphone diaphragm uses. Electrostatic coupling's specific power is limited by the base capacitance of the harvester, which is in turn limited by the dielectric constant of free space and the area of the conductors. For this reason, electrostatic harvesters generally have a much lower specific power than the other coupling mechanisms. However, electrostatic couplers are also mechanically very simple, and can be implemented using integrated-circuit MEMS designs, as in (Basset et al. 2009).

3.3.2 Modeling Kinetic Scavenging

We now discuss the general problem of selecting an inertial scavenging design for animal motion, given accelerometery data over multiple days of animal motion. Some research, such as (Aktakka, Kim, and Najafi 2011) or (Shafer 2013), focus on short intervals of consistent animal behavior, during which the animal's motion is particularly energetic. The consistency of behavior simplifies the design and analysis, and these devices result in high scavenging energy yields, but are not indicative of the viability of scavenging in long-term projects which include much longer periods of resting or light action.

The design space of inertial harvesters is large and many-dimensional. We can narrow this design space by first estimating the power that different approaches could gather. This requires modeling the harvesting system.

Throughout this section, we describe the position of the stator relative to the fixed earth frame as $y(t)$, and the position of the proof mass relative to the stator as $z(t)$. Except where noted, we focus on 1-D linear motion. Also note that we employ two distinct meanings of the word "linear." We refer to harvesters with linear *dynamics*, which are harvesters whose dynamics follow linear equations of motion (in other words, damped harmonic oscillators). We also refer to harvesters with linear *motion*, in which the proof mass slides on a linear joint [3], as opposed to rotating about an axis. A harvester can be linear in either, neither, or both senses.

Modeling harvesting dynamics

We begin with a general model of a 1-D linear harvester. In this model, as with all models discussed in this work, we assume that the motion of the stator is

[3] this also applies to cantilevers and pendulums, provided that the motions are small

unaffected by the presence of the harvesting mechanism, or in other words, that the stator has a mechanical output impedance of zero. We label the coordinate of the stator relative to the world as $y(t)$, and the coordinate of the proof mass relative to the stator as $z(t)$. The stator exerts a force on the proof mass consisting of two parts. F_L represents a mechanical force whose work cannot be directly captured, arising from gravity, friction, or the casing of the harvester. F_C is the an electrical damping force, whose work can be directly captured. We assume that F_L and F_C both depend on z and $\dot{z}$, though not necessarily in a linear way, and that F_C depends on the state of the harvesting circuit, which we model as a single variable, $v(t)$, representing the voltage on a storage capacitor.

The general equation of motion, then, satisfies the equation:

$$\ddot{z}(t) = \frac{\Big(F_L(z, \dot{z}) + F_C(z, \dot{z}, v)\Big)}{M_{proof}} - \ddot{y}(t)$$

The power available for scavenging is the mechanical work per unit time done by F_C on the proof mass, or

$$P_h(t) = -F_C \cdot (\dot{y} + \dot{z})$$

Not that $P_h(t)$ need not be positive. Conceivably, a harvester could expend energy to accelerate the proof mass when $(\dot{y} + \dot{z}$ is small, reaping greater benefits later when $(\dot{y} + \dot{z})$ has grown. This would represent a dramatic increase in the complexity of this problem, as well as in the electrical coupling circuit, and we know of no research that attempts this. In practice, the electrical circuit always rectifies the coupling's output, so F_C always opposes $(\dot{y} + \dot{z})$ and thus $P_h(t)$ is always positive.

In the animal-mounted domain, $y(t)$ is often quite complex, even during ap-

parently repetitive activities like walking or running. In addition, F_C and F_L are generally nonlinear with respect to $z, \dot{z}$, and v. Even very simple harvesting designs can exhibit chaotic behavior, as in (Spreemann et al. 2006). These functions can also be discontinuous, such as when z approaches the edge of its range of motion, when v is very low, or (in designs with sliding joints) when $\dot{z}$ is near the boundary between static and Culomb frictions.

As a result, the problem of modeling harvester dynamics from first principles is intractable for all but the most well-behaved harvesters. We now discuss some common simplifications, and experiment-based alternatives to dynamics modeling.

Resonant models

If we assume that the ambient motion is periodic, the analysis becomes much simpler. We can now establish an upper bound on the power that can be harvested from the motion. As (Yeatman 2008) shows, if the proof mass's range of motion is unconstrained, the maximum power is limited by:

$$P_{max,res} = M_{proof} \cdot \omega^3 Y_0^2 \tag{3.1}$$

Or, in the case that the amplitude of $\dot{y}$ is larger than the proof mass's range of motion, the smaller value

$$P_{max,res} = M_{proof} \cdot \omega^3 Y_0 Z_l \tag{3.2}$$

holds instead. Here, ω is the frequency of motion in radians per second, Y_0 is the amplitude of the vibrations in meters, and Z_l is the range of the proof mass's motion. This theoretical maximum is achieved when the proof mass transits across the full range of its motion at the moment of peak stator acceleration.

For rotational motion, the analogous equation is

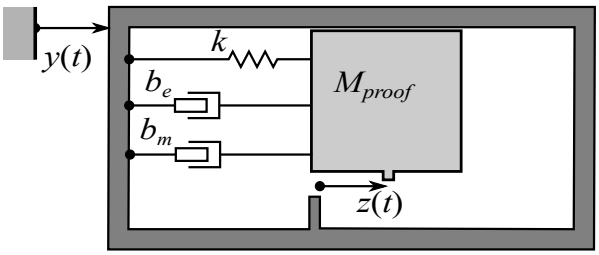

Figure 3.1: A kinetic scavenger as a simple harmonic oscillator

$$P_{max,res} = I_{proof} \cdot \omega^3 \Omega_0^2 \tag{3.3}$$

where I_{proof} is the proof mass's moment of inertia about its axis, and Ω is the amplitude of oscillation in radians.

Equations 3.1 - 3.3 assume a motion in which the proof mass makes a full transit at the moment of peak F_L, and then absorbs all of its kinetic energy in a negligible distance at the end of its transit. This motion is not physically realistic, although a hollow-tube design such as (Halim and Park 2014) or (Wijesundara et al. 2016) might approach this sort of motion under some circumstances. In order to achieve this generally, the scavenger would need to be able to exert some control on the proof mass, perhaps by holding the mass in place with a latch or magnet before releasing it at the optimal moment.

A more common design attaches the proof mass to a spring or cantilever. This creates a damped harmonic oscillator. The damping force is typically modeled as the sum of a mechanical damping force arising from friction, and an electrical damping force from the coupling mechanism.

As (Roundy, Wright, and Rabaey 2003) demonstrates, the maximum average power that such a harvester can gather from sinusoidal motion is

$$|P| = \frac{m\zeta_e}{4(\zeta_e + \zeta_m)^2}\omega^3 {Y_0}^2 = \frac{m\zeta_e}{4(\zeta_e + \zeta_m)^2}\frac{A^2}{\omega}$$

This result occurs when the natural frequency of oscillator matches the ambient periodic motion (that is, when $\omega_{ambient} = k/M_{proof}$. Note that at this frequency, the amplitude of the proof mass's motion is larger than the amplitude of the ambient motion. Also note that the assumption of linear dynamics requires that the proof mass can move over the full range of this motion.

This result suggests a general design procedure for designing a resonant harvester: First, choose a mechanical design that minimizes ζ_m, and then construct a circuit to make $\zeta_e = \zeta_m$. In practice, ζ_m depends on load conditions, so this step can be achieved as part of maximum power-point tracking circuitry, as we discuss later.

Another design parameter to consider is the quality factor, $Q = 1/(\zeta_e + \zeta_m)$. If the peak frequency of the ambient vibrations is known, this should be set as high as possible. However, if the peak frequency is likely to vary within a range, Q could be intentionally decreased. This would decrease the harvester's efficiency at its resonant frequency, but increase its efficiency at nearby frequencies, increasing the "bandwidth" of the harvester.

Pendulum Models

Equation 3.3 assumes that all proof mass torques come from the stator's rotation in the world frame. It does not describe the influence of gravity, or of linear stator motion, both of which can create torques in the proof mass. For this reason, rotational scavengers often use half-disk proof masses, which maintain high proof moment-of-inertia while also allowing large torques from gravity and linear motion, as long as those accelerations are perpendicular to the proof masses

position.

(Yeatman 2008) provides newtonian analysis of half-disk pendulums under linear-dynamics damping, which appears to be a reasonable model for a Sieko Kinetic wristwatch [4]. Yeatman's analysis finds that, in non-resonant operation, an ideal half-disk generator can scavenge approximately

$$P_{linear-to-rotational} = \frac{1}{2} M_{proof} \omega^3 Y_0 Z_1 R$$

from linear motion, where R is the radius if the proof disk. In non-resonant operation, an ideal half-disk generator is approximately as effective as a linear generator for harvesting linear motion, under the condition that the amplitude of the motion is small compared to the radius of the proof disk, so the oscillations of the proof disk are small. This implies that a rotational scavenger could, in principle, effectively scavenge energy from both rotational and linear motion, though not necessarily at the same time.

(Pillatsch, Yeatman, and Holmes 2014) and (Xue et al. 2014) experimentally test the resulting equations of motion using up-converting harvesters. However, as Xue and Pillastch both find only hundreds of microwatts of power in wrist-mounted generators, since the moment of inertia of these proof masses is small, and the oscillation amplitude is limited on human wrists.

Non-resonant models

One common approach to modeling non-resonant models is to simply ignore the non-linear behavior, and assume that the harvester's response to a broader spectrum can be calculated using the sum of its responses at lower frequencies. The harvester is subjected to sinusoidal motion at a range of frequencies, and

[4] See the experimental results in this section for a discussion of observed behavior that may defy this model

its response is recorded, resulting in a specific power vs frequency curve. This approach is identical to the approach used for linear harvesters, albeit with more dubious applicability to wide-spectrum motion, or even narrow-spectrum motion at different amplitudes.

An alternate approach avoids detailed modeling and instead measures the generator's response to a benchmark: Attach the harvester to a human at one of several locations, typically wrist, waist, and ankle. The human, often the first author, will run at various speeds. As a standard, this method has flaws, since the results depend in part on the runner's body and physique. On the other hand, this test is relatively easy to perform, and does capture a complex, organic motion that humans are likely to engage in. The use of the word "model" may seem like a poor fit for these phenomenological measurements, but they do implicitly assume that the test subjects are reasonable proxies for general human behavior, even if the precise physics of the test subjects are mostly hidden.

A few examples of harvester tested with the treadmill benchmark are (Bowers and Arnold 2008), (Mitcheson et al. 2008), (Ylli et al. 2015), (Donelan et al. 2008), and (Granstrom et al. 2007). (Wahbah et al. 2014) uses a similar approach for a wrist-mounted cantilever, measuring power generation over the course of daily activities.

A more replicable approach, advocated by (Gorlatova et al. 2014), is to record characteristics of the runner, and then reproduce that motion in a controlled stage. (Xue and Jin 2010) has recorded a large dataset of running humans, which Gorlatova uses in testing their own kinetic harvester. (Yun et al. 2011) uses this approach as well, and (Choi et al. 2011) uses a similar strategy, but reduces human motion to a few frequency components, presumably to simplify replication.

The "human on treadmill" benchmark may be useful in designing for pumas,

as well, since the walking spectrum of pumas is comparable to that of humans.

3.3.3 Kinetic Scavenging in Pumas

Our first step in determining the design of a puma-mounted kinetic scavenger is to assess the possible energy that can be captured in a puma, and identify components of the puma's motion that are most valuable for harvesting. To do this, we analyzed a 24-hour window of accelerometery data from (Wang et al. 2015). The data was broken into 4-second windows, and each window was decomposed into its spectral components using a discrete Fourier transform. This allowed us to assemble a 2-D histogram representing the average rate at which the puma exhibited each frequency and magnitude. Each frequency-magnitude pair in this histogram can generate a power-per-mass proportional to $y_0^2\omega^3$, which we call the "raw" specific power of that region of frequency-vs-amplitude space. Then, the average specific power available at each region of frequency-vs-amplitude space is the element-wise product of the normalized histogram and the raw energy map. The results of this analysis are given below for the X-axis, which was found to have the highest overall specific power of the three axes.

This analysis shows a specific power on the order of 2 watts/kg for some components of motion. The collar described in in (Rutishauser et al. 2011) weighed about 450 g. If the mass were totally dedicated to proof mass, an ideal 1-D resonant linear-motion harvester could scavenge a maximum usable power on the order of watts.

However, these components have an oscillation amplitude on the order of meters, requiring a stator far longer than a mountain lion can be expected to tolerate. In this case, we instead should use equation 3.1. We assume a proof mass range of 1 cm in Figure 3.3, as this is on the order of the length of a tag's housing.

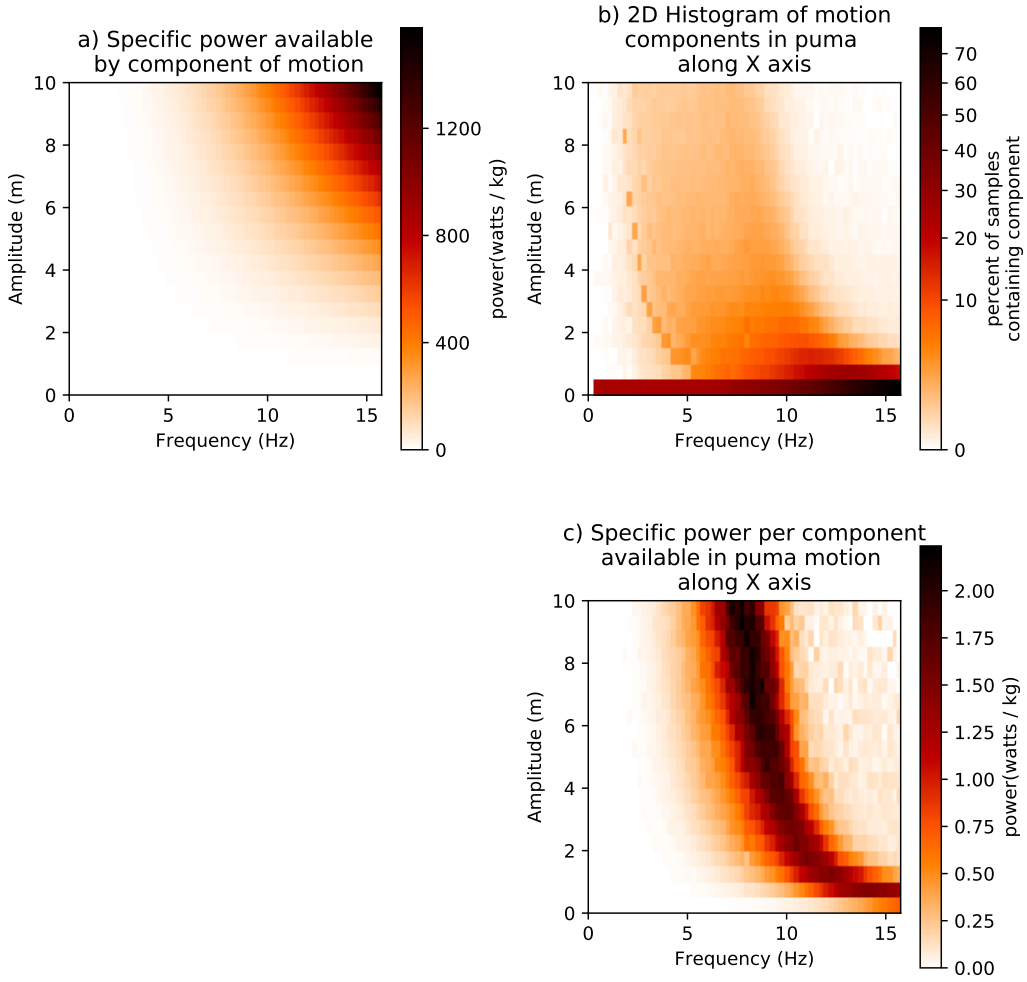

Figure 3.2: A per-component analysis of the maximum specific power available to harvest in motion along the X-axis from a puma in (Wang et al. 2015). a) The specific power available at each amplitude and frequency, as described by equation 3.1. b) The density of components in puma motion over a 24-hour period. Data is given as a fraction of overall time, so the sum of the bins in each column is 100%. c) The specific power available to harvest at each frequency and amplitude. This plot is the element-wise product of the two upper plots.

In this case, the constraint lowers the maximum harvestable power by a factor of about 20.

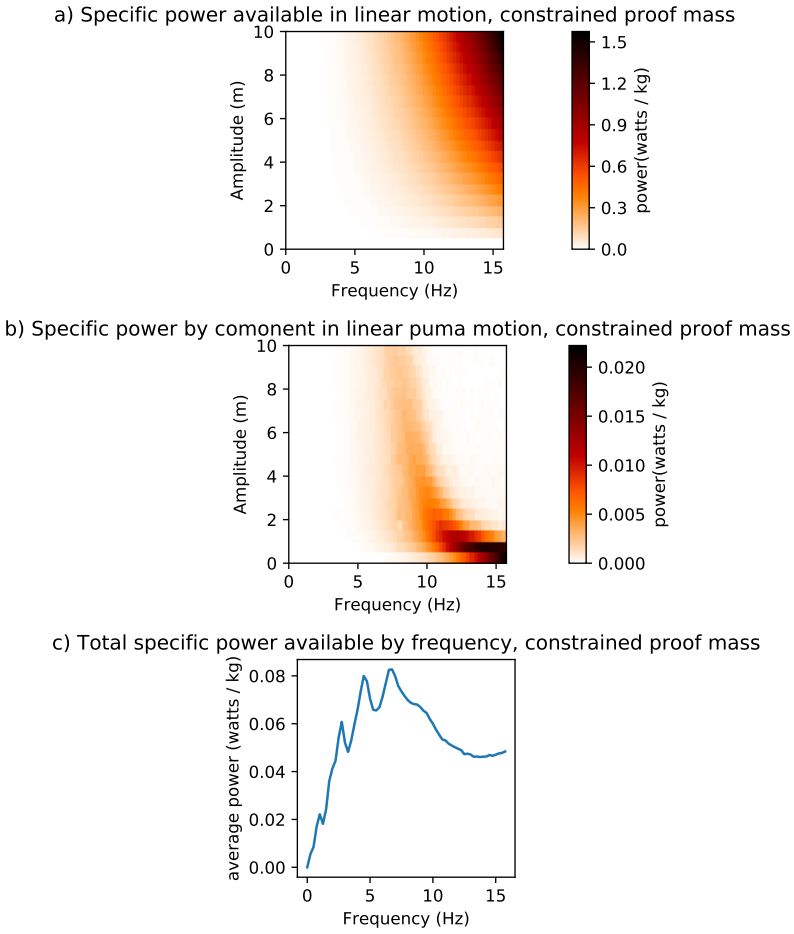

Figure 3.3: A per-component analysis of the maximum specific power available if the motion of the proof mass is constrained, as described by 3.2. a) shows the raw specific power available in linear motion when the proof mass is constrained to 1cm. b) shows the power per component available in linear puma motion, given these constraints. c) shows the specific power available by frequency. It is the total of each column in graph b.

We also consider harvesting from rotational motion. Our dataset did not include gyrometery, so we do not have a direct measurement of the rotational motion a mountain lion tag undergoes. However, we can use an indirect measure to infer the angle of inclination of the tag using gravity, which accelerometers do

capture. The general procedure is described in (Mizell 2003).

This measure is at best only useful as a rough estimate, since signals due gravity cannot be generally distinguished from signals due to acceleration in the world frame, but can still provide a rough guide for designing a kinetic harvester. The results of this analysis are illustrated in Figure 3.4.

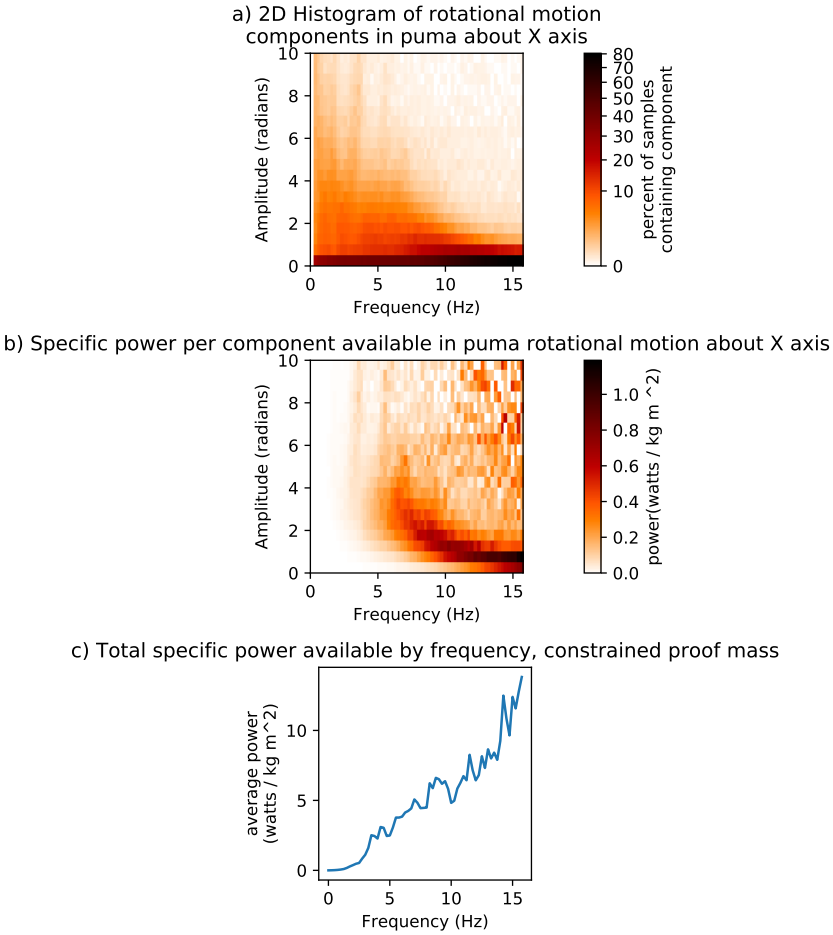

Figure 3.4: A per-component analysis of the power available for scavenging in rotational motion, as described by 3.2. a) shows the raw specific power available in linear motion when the proof mass is constrained to 1cm. b) shows the power per component available in linear puma motion, given these constraints. c) shows the specific power available by frequency. It is the total of each column in graph b.

The moment of inertia of a half-disk is $1/2MR^2$, which we estimate to be about

$10^{-6} kgm^2$ for the Seiko Kinetic's proof mass, so an unmodified collar-mounted Seiko Kinetic could perhaps harvest on the order of microwatts.

This analysis suggests that there is very little ambient energy available in the motions of a mountain lion's neck. If accurate, this is perhaps unsurprising. Mountain lion physiology produces mostly low-frequency motion, optimizing energy conservation. This is in contrast to vibrations of automobiles and HVAC systems, whose designs are more typically aimed at manufacturing convenience and effectiveness, tending to waste more energy.

3.3.4 ESCAPE Kinetic Scavenging Designs

We tested three designs for kinetic scavengers.

Our first design was a simple piezoelectric cantilever, using an off-the-shelf cantilever from SparkFun electronics. This design was attractive because of its apparent simplicity and low cost. To tune the natural frequency of the piezoelectric, a fine piece of spring steel was added along the cantilever, similar to the design in (Shafer and Morgan 2014). The proof mass was a magnet, allowing easy adjustment by adding washers. In theory, this resulted in an adjustable linear scavenger. In practice, the natural frequency was very hard to tune, and even when tuned, the proof mass's oscillations were only resonant under very small motion components. We also attempted a frequency up-converter using a magnetic plucking arrangement similar to (Pillatsch, Yeatman, and Holmes 2014), but were unable to produce up-conversion reliably.

Our second design used the mechanism (called a "movement") of a Sieko Kinetic wristwatch, following (Goto, Sugiura, and Kazui 1998). The Seiko Kinetic was chosen because it is built to capture human motion, which is reasonably similar to puma motion in spectral decomposition. The movement was carefully disas-

sembled, and all timekeeping components were removed. The harvesting inductor was then re-soldered to a pair of fine wires which were fed through a convenient hole in the casing. We also constructed a cage that allowed attaching additional weights to the Seiko Kinetic's pendulum to increase its moment-of-inertia.

A third design was a faraday-coupled generator built using a brushless-DC motor, on the assumption that an efficient electricity-to-torque transducer would also allow efficient torque-to-electricity transduction. A half-disk pendulum was attached to the shaft, and an adjustable spring was attached to the stator. By adjusting the compression of the spring, its effective spring constant could be altered, allowing tuning of the oscillator's natural frequency.

We also constructed two types of rectifier to convert the AC output to DC. The first was a typical 4-diode bridge using low-drop GaAs diodes. The second was an active rectifier following (Sun et al. 2011), constructed using the ultra-low current Texas Instruments TL331 comparator and low-drop MOSFETs.

Laboratory Testing

To explore and refine our kinetic scavenger elements, we first constructed a pair of test gantries to simulate the motion of a mountain lion's tracking collar. Both gantries control a stage with 1 degree of freedom. The stage of one gantry moves linearly, while the other rotates about an axis. Encoders provide feedback, and a simple control loop controls the stage.

We tested each of three types of scavengers on each stage, using a sample of accelerometry data from puma treadmill experiments in (Bryce 2017) as the control signal. Each output was observed in open-wire condition, and was also used to charge a capacitor whose voltage was recorded over time.

On the linear stage, no harvester produced significant output. The output of

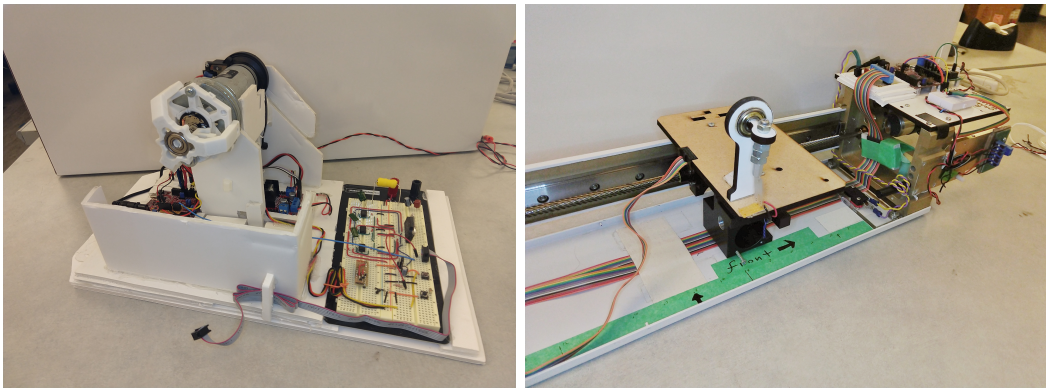

Figure 3.5: Linear and rotary test stages.

the piezoelectric harvester and the BLDC harvester was below 1mV. This is not unexpected, since the motion of both harvesters matched the dominant frequency of the mountain lion's walking, at about 1.5 hZ. The Seiko Kinetic harvester's pendulum was constrained by static friction, and rarely moved with respect to the stator. When it moved, it produced bursts as high as 1.2 v, but only occasionally, so the rate of charge was not significant.

On the rotary stage, the piezoelectric and brushless-DC generators again produced negligable output. However, the Sieko Kinetic moved more freely, and produced a measureable output. The results of the capacitor-charging experiment are shown below using a passive and an active rectifier:

We also examined the result of altering the Seiko Kinetic's proof mass. The proof moment-of-inertia was approximately doubled by adding weights to the cage.

Note that both of these records were taken from logs in which the storage capacitor's size may have been recorded incorrectly. The capacitor may have been a 10uF capacitor, in which case these results should be divided by 10.

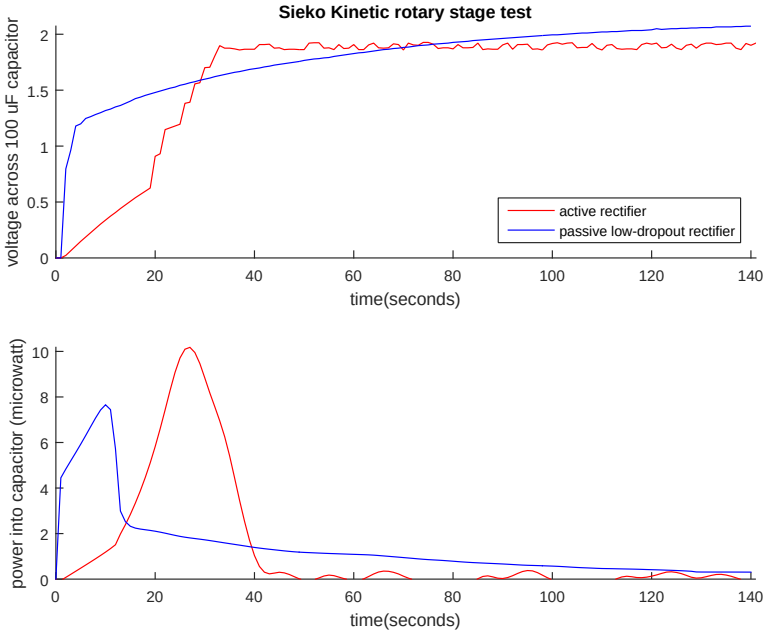

Figure 3.6: Results of testing Seiko Kinetic scavenger on rotational stage, simulating puma walking motion

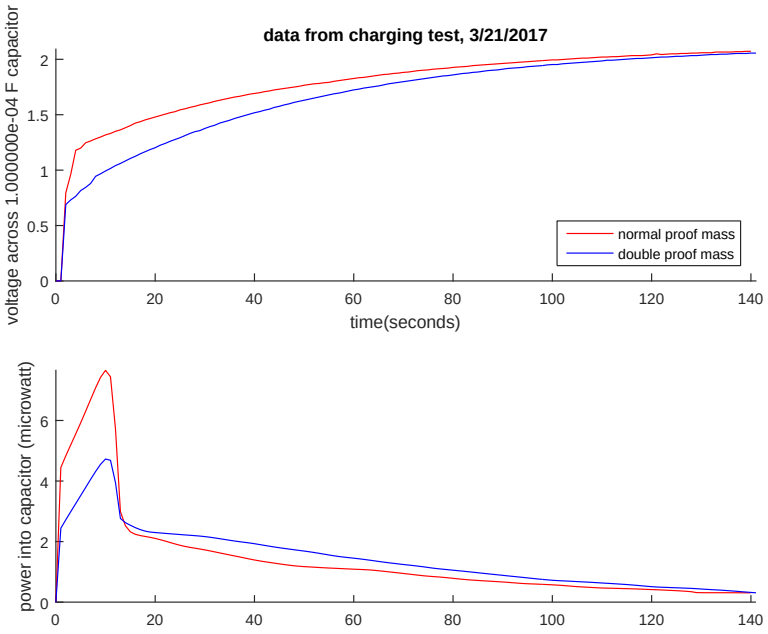

Figure 3.7: Results of testing Seiko Kinetic scavenger on rotational stage, altering proof mass

3.3.5 Discussion of kinetic scavenging in mountain lions

While theoretical analysis does suggest a significant specific power in the linear motion of a mountain lion's collar, this power can only be obtained by utilizing a large portion of the collar's hardware. This is infeasible for the electronics payload, or at least the portion containing the accelerometry unit and heat scavenger. The battery pack, however, could be effectively leveraged as a proof mass. Even so, this presents significant hardware challenges. It is not clear what kind of coupling mechanism could effectively couple a proof mass at that scale.

The results from the rotational tests present an interesting puzzle. The Seiko produced a maximum of about 10 uW. This is actually about one to two orders of magnitude *larger* than the theoretical maximum predicted by equation 3.3. One possibility is an error in the recording setup. Since other errors have been found, this is plausible.

A second possiblity is that the assumptions used to derive 3.3 do not apply to the Seiko Kinetic. In particular, we noticed that the Seiko pendulum is very sensitive to static friction, which appears to be a benefit in some situations and a detraction in others. Under slow, large oscillations, the static friction allows the pendulum to rise to a nearly horizontal angle before dropping. Under this regime, the motion of the stage is doing work against gravity to store potential energy, which is captured as kinetic energy later. This is an entirely different paradigm of energy capture than the inertial scavenging discussed so far. This phenomenon merits further investigation.

Increasing the proof mass apparently reduced the power produced by the Sieko Kinetic harvester. Again, this contradicts 3.3. One explaination is that the added proof mass increased the mechanical friction of the proof mass, decreasing conversion efficiency. Another explanation is that the proof mass prevented static friction

from producing significant potential energy, again meriting further investigation.

While the Sieko Kinetic's physical behavior is interesting, it seems unlikely that a rotary scavenger is likely to significantly offset the tag's power consumption. The combination of small oscillation amplitudes and small proof mass dimensions reduce the efficacy of a rotational harvester.

In principle, these results could be improved by increasing the moment of inertia of the proof mass. One proposed design, shown in (Wu et al. 2014), proposes using a large external pendulum as a proof mass. By breaking the bounds of the tag enclosure, this increases the moment of inertia by several orders of magnitude, and increases the linear range of the proof mass as well. However, it does so by dramatically altering the form factor of the collar in a way that severely impacts its robustness and would surely be distracting for the animal. Another approach could use the batteries (which often comprise a majority of the mass of the tag) as the proof mass. However, as the proof mass increases, the reactive force from the proof mass will start to move the collar, and would impact accelerometry readings. Also, experience with designing these harvesters suggests that this force would be distracting for a tagged animal.

In considering the efficacy of a scavenging device, we must also compare its utility to its opportunity cost. One reasonable point of comparison is the specific energy of a primary battery, which could take the scavenger's place in a tag. In the case of the puma, we found a maximum specific power of about 0.08 watt/kg. If we assume a tag lifetime of about 2 months, this yields about 120 watt-hours/kg. A lithium-thionyl chloride battery has a specific energy of about 500 watt-hours/kg, and even a generic alkaline battery carries about 80-180 watt-hours/kg.

In summary, it seems unlikely that even an unrealistically efficient kinetic harvester could produce more energy over the lifetime of a tag than could be added

to the collar by removing the kinetic harvester and using the extra mass to increase the size of the battery. It is possible that a kinetic scavenger could be useful on a more energetic animal, or on a tagging mission with a long intended lifespan, but even then this approach presents significant hardware design challenges.

.

3.4 Other Types of Energy Scavenging

3.4.1 Solar Scavenging

Solar panels are devices which convert energy in the form of light into electrical currents. The key technology is the photovoltaic cell, which uses a thin film of one metal plated over a substrate of a second metal. If the metal of the thin film has a different free electron density than the substrate, then a depletion zone forms between them, forming a barrier to electron flow. Photons absorbed near the depletion zone scatter electrons, some of which cross the barrier. Since there are more free electrons on one side of the barrier than the other, the net effect is a current flow across the barrier, which can be directed through a circuit elsewhere. This phenomenon was first observed in 1839, but early solar cells were highly inefficient, producing miniscule currents in direct sunlight. Useful solar cells required the innovation of doped semiconductors, as pioneered by Bell Labs in the 1950s.

The production of solar cells was motivated by the desire to build spacecraft. The first such device was Vanguard I in 1959, which used six tiny solar cells to augment its small non-rechargeable battery. Vanguard I transmitted signals for six years after its launch, far outlasting its non-scavenging predecessors and demonstrating the feasibility of solar scavenging in space.

We consider the application of this technology to another hermetic embedded system: wildlife tags. Spacecraft have the luxury of a predictable and mostly unobstructed line-of-sight to the sun. On the surface of the earth, systems must contend with weather, dirt, the atmosphere, landscapes, and nighttime. Also, wild animals cannot be expected to maintain the cleanliness and optimal positioning of their collars. In spite of all these challenges, the intensity of solar radiation that reaches the surface of the earth is still quite high, and so remains an attractive option.

Prior Art

(Patton, Beaty, and Smith 1973) first tested a solar panel on a single wild turkey. In this experiment, the panel was used as a replacement for a battery in a radio transmitter, although the authors suggest that a solar panel could be used to recharge a battery as well. (Church 1980) applies this technique to gray partridges, noting significant gains in longevity. (Andersen 1994) provides detailed longevity statistics in a study of red-tailed hawks, using solar panels and nickel-cadmium batteries. These tags showed clear and dramatic improvements in longevity, and one tag remained operational for seven years. Solar panels are now mainstream in avian tracking (MacCurdy et al. 2008), (Wu et al. 2014).

Though solar panels are fairly common for avian trackers, there has been comparatively less investigation and deployment of solar-scavenging collars for wild terrestrial or marine animals. (Zhang et al. 2004) designed a generic solar collar for the ZebraNet system. Their solar array produced about 0.4 watts/100g in full sun, though they do not report the on the efficacy of this approach in the field. (Adoram-Kershner et al. 2017) used a laboratory prototype to examine the feasibility of solar tags on elephant seals, and concluded such an approach could

be viable.

(Wilson et al. 2013) designed a solar-scavenging collars for wild cheetahs. This paper used an array of solar cells, reporting a current production that ranged from 35 mA in direct sun, 10 mA in dappled shade, and near zero otherwise, averaging about 2mA over time. The authors note that the cheetahs apparently spend very little time in the sun, even during winter. These same collars were deployed on African wild dogs in (Hubel et al. 2016), though detailed power data was not reported.

Perhaps most notably, (Jurdak et al. 2013b) and (Sommer et al. 2016) utilize solar cells in their Camazotz tags for wild flying foxes. They report that these tags, used in combination with aggressive energy conservation techniques, are approximately energy-neutral. Early trials in (Jurdak et al. 2013b) suggest as much as 5.7 mW average power can be produced by a a pair of approximately 1 in^2 panels. (Sommer et al. 2016) deployed these tags for long term trials, harvesting an average of 1.137 mA over a day, presumably measured over a 3.6v circuit for an average power generation of 4 mW. Since their tags drew 1.3 mA on average, this fell slightly short of true energy neutrality, although nearly half of days did achieve energy neutrality. In this case, increasing the ratio of rechargable battery mass to non-rechargable battery mass would have been advantageous.

Applicability to Puma tags

We begin by estimating an extremely optimistic upper bound on solar scavenging. The intensity of solar radiation at the surface of the earth is approximately 1120 W/m^2 at the sun's zenith, including indirect rays from the atmosphere. Sunlight is only available during about half of each day, during clear weather. Consumer solar cells have typically about 25% conversion efficiency, under ideal

conditions. On one test collar, the top side of the tag enclosure was about 2x3 inches. A highly efficient solar cell, mounted on this enclosure, could produce no more than 500 mW averaged over a day, well over the power consumption of most tags.

Of course, such a result is highly implausible, since weather and puma behavior will both prevent ideal conditions. At present, we cannot find any sort of research that might allow an estimate of a puma's daily light exposure, although perhaps the behavior of cheetahs in (Wilson et al. 2013) is suitable. Adding a solar cell to the ESCAPE tags would present an opportunity to evaluate this, since solar panels also double as light sensors.

Implementing Solar Panels

Solar panels should probably be attached to the top face of a collar, where sunlight is most likely to be incident. Solar cells are thin and fragile, but may be enclosed in glass, plastic, or epoxy casings, at the cost of efficiency. This would be feasible for mounting on top of an enclosure. Possibly, the band of the collar presents an opportunity for more surface area, and thus more power, although mounting a cell in a collar band without detracting from its stability presents a challenge.

3.4.2 Thermal Scavenging

Another form of energy scavenging is thermal scavenging. Any temperature difference across the surface of an object can be used to capture useful energy, at least in principle. In the nineteenth century, this facet of thermodynamics was the motivating principle behind mechanical heat engines such as the Stirling engine and Carnot engine. Today, the heat scavenging mechanism of choice is a

compact and inexpensive solid-state device called the Peltier Electric Generator, or PEG. The PEG leverages a thermodynamic phenomenon called the Peltier-Seebeck effect, in which the junction between two different metals exhibits a small, temperature-dependent voltage. If a circuit crosses different types of metal, and one junction is at a higher temperature than another, the result is a slight voltage difference between the junctions which creates a slight current in the circuit. The PEG sandwiches many such junctions between two thin ceramic plates, wired together in series so that the slight voltage difference is multiplied into a larger voltage and current. This increases the power a PEG can generate, but also increases the rate at which heat energy dissipates from the hot side (Kiely et al. 1991).

Two parameters are particularly important in assessing the viability of a Peltier TEG in a thermal harvesting system. The most important is the "figure-of-merit", commonly denoted Z, and defined as

$$Z = \frac{(\alpha_p - \alpha_n)^2 \sigma}{k}$$

where α_p and α_n are Seebeck coefficients of the p- and n-type semiconductors, σ is the electrical resistivity of the semiconductors, and k is the thermal conductance of the semiconductors. Z is a property of the semiconductor choice, and is particularly crucial because the power generated by a TEG is approximately proportional to Z, and because this parameter is a factor in electrical load-matching during harvesting (Bhandari and Rowe 1995). A common material for TEG construction is bismuth-telluride, with a room-temperature Z of about $0.0066K^{-}1$.

A second crucial parameter is the "empty" thermal resistivity, often denoted R_{empty}. This is defined as $R_{empty} = \Delta T_{TEG}/W_{TEG,empty}$ in (Leonov 2011), where $W_{TEG,empty}$ is the heat flow that would cross the wafer at a given temperature,

if the semiconductors were removed. It is determined by the material properties of the wafer, and by its geometry. This parameter is important because it guides design choices in the geometery of the TEG system, as discussed in the section on TEG optimization.

TEGs can be mounted in a variety of ways. The wafer can be sandwiched between heat sinks to change the effective shape of the generator, so forms like buttons (Hoang et al. 2009) and coins (Stark 2006) are possible. (Settaluri, Lo, and Ram 2012) creates a large u-shaped brace that wraps around a human arm. (Leonov 2013) fashion several designs, including antannae and crowns. Semiconductor junctions can also be woven into fabric (Kim et al. 2014) to create flexible TEGs, though this performs below the efficiency of a rigid ceramic wafer.

3.4.3 TEG modeling and optimization

TEG efficiency is usually modeled using a "thermal circuit" analysis. Leonov outlines this procedure in (Bonfiglio and Rossi 2011), and this technique is applied to practical thermal harvesting systems in, for example, (Hoang et al. 2009), (Kim et al. 2014), and (Leonov 2013).

Thermal circuit models are analogous to electrical circuit models, substituting electrical current with thermal energy current, and voltage with temperature. The TEG capture system is the load resistor, R_{TEG}, and the difference in temperature across it is proportional to V_{TEG} in the real electric circuit. The air and the body core are taken as fixed sources and sinks, T_{air} and T_{body}, and the thermal transfer coefficients of the heat sinks and skin are constant resistances, R_{TEG} and R_{skin}. More detailed models would include resistors representing parasitic heat loss, and might handle dynamic effects with capacitors. For most purposes, though, a three-resistor model is sufficient.

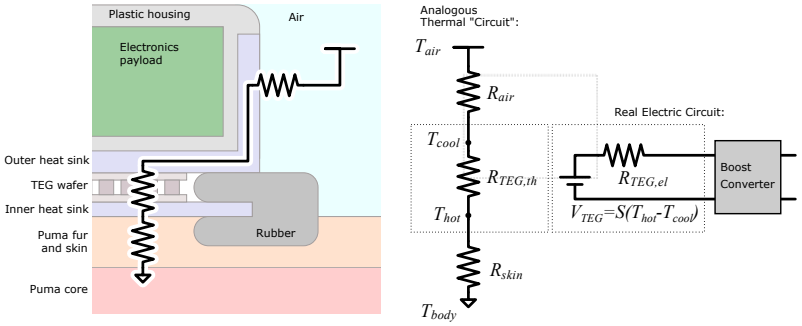

Figure 3.8: Three-resistor thermal model of a collar-mounted TEG. The diagram represents a sagittal cross-section of a puma wearing a collar and tag.

Under this model, we can see that performance is improved by minimizing resistors R_{skin} and R_{air}. Both R_{skin} and R_{air} are functions of the heat-sink geometry. Large surface areas reduce thermal resistance, as do protuberances which promote convection. R_{skin} varies between different locations on the body, reflecting differences in bloodflow, fat, and hair. R_{air} is reduced in the presence of convection currents.

Once R_{skin} and R_{air} are minimized and modelled, an optimal TEG can be chosen. Assuming the electrical harvesting circuit is optimally load-matched, the power that a thermopile can generate is given by (Freunek et al. 2009) as

$$P_{max} = \frac{\Delta T^2}{4} \cdot \frac{Z\sqrt{ZT_0+1}}{(R_{skin}+R_{air}) \cdot (1+ZT_0+\sqrt{ZT_0+1}) \cdot (1+\sqrt{ZT_0+1})} \tag{3.4}$$

where W_{TEG} and ΔT_{TEG} are the heat flow and temperature difference across the thermopile. This is analogous to the electric-circuit $P = IV$, which implies that optimal TEG design requires thermal load-matching as well as electrical load matching. $R_{TEG,th}$ changes by as much as a factor of two (Leonov and Fiorini 2007) with generated electric current, so these matching problems are not independent.

The analysis becomes quite complicated, and different authors have come to different conclusions as a result of different assumptions and simplifications. For example, (Freunek et al. 2009) finds that optimal electrical load-matching requires $R_{load} = R_{TEG,el}$, and optimal thermal load-matching occurs when the height-to-cross-sectional-area ratio, l/mA, of the TEG semiconductors is $S^2 \cdot (R_{skin} + R_{air}) \cdot \sqrt{ZT_0 + 1}$. (Leonov 2011) suggests this ratio should always be as high as possible when optimizing for power-per-volume or power-per-weight. However, in practice, designs are often guided by spatial constraints. In our analysis below, we assume we will use a single wafer, which simplifies the analysis considerably.

Applicability to Pumas

Here again, the particular domain of animal-mounted devices places severe limits on the utility of energy scavenging devices. The laws of thermodynamics state that the maximum usable energy that a thermoelectric harvesting device can produce depends on the temperature difference between the hot and cold side of the device. Furthermore, animals' skins generally insulate their internal, temperature-regulated bodies from the outside world, further limiting the efficacy of such devices.

One interesting advantage to using this technique on puma collars is that a collar's form factor is already an excellent heat sink geometry. The interior of the collar is a large surface area, and the electronics enclosure protrudes into the air. R_{air} would be minimized by using a metal enclosure, though in practice we would leave a plastic section to allow GPS antennas a free view of the sky. R_{skin} could conceivably be reduced further with metal combs that burrow into fur.

To estimate the potential of TEG harvesting in this application, we first must model R_{skin} and R_{air} for a puma. These parameters are notoriously hard to model

in humans, with the former varying widely with position on the human body and the latter varying widely with the geometry of the TEG and the body (Leonov and Fiorini 2007). However, we can obtain a very rough estimate of this parameter by simply dividing the time-averaged core-to-air temperature differential by the average energy generation rate of the puma, implicitly assuming a spherical puma with uniform skin and fur.

(Laundré 2005) estimates the energy generation rate at around 2500 kcal/day, or about 120 watts. (McNab 2000) measures the internal temperature of several pumas, and reports a typical 38 deg C. The 36M data from (Wang et al. 2015) records a typical average external temperature of about 25 deg C. Thus, a rough estimate of $R_{skin} + R_{air}$ for a puma is about $R = \Delta T/W = (38-25)K/120watt = 0.1K/watt$ for its entire skin. If our spherical puma has a radius of half a meter, then its surface area is about $10m^2$, so the approximate thermal-resistance-per-area is about $.01K/wattm^2$. We assume we are using a typical bismuth-telluride peltier module, with a Z of about 0.0066 K^{-1} at room temperature.

Then, according to the optimum power formula in equation 3.4, we have a roughly estimated power-per-area output of about 3 W/m^2. A TEG mounted in the bottom of a 2x3 inch tag enclosure could conceivably draw about 10 mW. This estimate is not necessarily an upper bound: Effective heat sink design could probably lower $(R_{skin} + R_{air})$, which would raise the power generation rate. However, we would be unlikely to achieve the optimal harvesting geometry, and boost conversion requirements would prevent us from achieving ideal TEG load-matching. In any case, this amount is on the order of energy scavenged from other types of devices, and so is worth exploring.

Chapter 4

Adaptive GPS Sampling

The ability to perform location tracking is a core motivation behind wildlife tagging technology. Tracking yields information about migration, foraging habits, physiology, and social behavior, an provides useful guidance for conservation efforts (Wilmers et al. 2015), (Mech and Barber 2002). This capability was previously achieved using the radio transmitters on board the collar. Ground stations and researchers could measure the signal's direction and estimate its distance. From this information, the transmitter's latitude and longitude can be calculated. This method works, but ground stations and researchers are expensive, often imprecise, and generally limited in the territory they can cover.

A GPS-equipped collar, however, can measure its own latitude, longitude, and (provided it can read the signals of four or more satellites), height above sea level. Depending on satellite visiblity and power use, a GPS receiver can localize with a precision of ± 5m ((D'Eon and Delparte 2005),(Bauer 2013),(Moriarty and Epps 2015)). GPS is a powerful tool for tracking, but it comes at a price: measurements are highly energy intensive. Various designs devote 31%, 32-79%, 39%, 45%, and 80% of their energy budget to GPS receivers((Jurdak et al. 2010), (Jurdak et al. 2013a),(Jurdak et al. 2013b), (Dunne 2014), and (Rutishauser et al.

2011) respectively). When (Wilson et al. 2013) reduced the GPS sample rate on some collars from 30s to 300s, the result was a 30% overall power reduction.

As with any sensor, there is a trade-off between GPS measurement frequency and the information gained from the sensor. A measurement is a purchase, exchanging energy for information (Bhattacharya and Das 2002; Brown et al. 2012). Removing measurements from the schedule will save some joules, but cost some information.

However, not all measurements are created equal: The costs and benefits of measurements can vary, so a careful strategy can avoid the most costly measurements, or ration energy for the most information-rich measurements. In this section, we explore the state of the art of these adaptive sampling strategies, and present and test our own strategy.

It is important to note that any adaptive sampling strategy requires some sort of predictive model. We can view an adaptive sensing strategy as a lossy compressor, and the loss rate and compression ratio of lossy compression depend on the predictive capabilities of a model.

Our search for models that shape a sampling strategy borrows heavily from the literature on Personal Communication Service (PCS) devices, a family that includes mobile phones and wearables. This field faces similar design goals and constraints, aiming to perform tracking of a moving animal while conserving battery life.

We categorize adaptive GPS localization strategies into four types: Mode-based strategies note that animal's behavior often falls into one of a handful of modes, such as resting, traveling, and hunting, each requiring different levels of measurement frequency. Context-based strategies estimate the likely cost and quality of a measurement to favor cheaper or more precise measurements. Place-

to-place models observe that animals often prefer certain places, and focuses measurements on transitions between these places. Finally, uncertainty suppression strategies model location as a probability density function, and schedules measurements to keep the spread of this density above a threshold.

As (Brown et al. 2012) points out, there is a core challenge facing any animal tracking project that uses mobility predictions. The mobility model must be built using existing data, but often what ecologists hope to observe is *changes* in animal behavior, or unusual behaviors. After all, if a model can perfectly predict an animal's behavior, then no collar is necessary. Any tracking project that wishes to use adaptive power consumption carries a risk that the model will miss crucial behaviors that defy the model. Therefore, sampling policy should be constructed in a conservative way, erring on the side of too many measurements.

4.1 Review of strategies for adaptive sampling

We broadly categorize existing adaptive sampling strategies for animal tracking into three broad categories: Mode-based strategies classify animal behavior into one of several discrete modes, where each mode has a different power policy. Context-sensitive GPS sampling uses other available information about the tag's environment or state to guide its sampling schedule. And finally, uncertainty suppression attempts to estimate the tag's location, and triggers GPS measurements when the uncertainty about the tag's location exceeds some threshold.

4.1.1 Mode-based strategies

When animal movement is observed over long periods of time, their motion seems to cluster into a set of behavioral states. For example, (Morales et al. 2004)

classifies elk movements into ”encamped" and ”exploratory" states, (Martiskainen et al. 2009) sorts cow behavior into eight behaviors including ”ruminating" and ”lame walking". (Wang et al. 2015) categorizes wild pumas as ”feeding", ”grooming", ”resting", ”high-acceleration", and ”low-acceleration". The modes are not limited to activity: (Janis, Clark, and Johnson 1999) finds captive pumas engage in ”lying",”walking", ”standing", and ”sitting", and a negligible amount of ”running".

Since animals change their states infrequently, knowledge of an animal's state allows prediction of the animal's future movements. A sleeping animal is unlikely to move soon, so a GPS measurement can be deferred. (Jurdak et al. 2013a) uses this strategy to manage GPS measurements in a tag for flying foxes. These tags use inertial measurements, solar sensors, audio signals, and air pressure to characterize the animal's state. GPS measurements are frequent while the animal is flying, less-frequent while resting, and event-triggered by certain actions. Similar strategies are emploted in (Wilson et al. 2013) and (Brown et al. 2012).

4.1.2 Context-sensitive GPS Sampling

GPS measurements do not have uniform costs. Two factors in particular affect the energy cost (and, sometimes, the resulting accuracy) of a GPS measurement.

First, GPS receivers must maintain information about the trajectories of GPS satellites. Coarse ”almanac" data is valid for several weeks, while the fine-tuning ”ephemeris" data is valid for 1-4 hours (Moriarty and Epps 2015). Fix success rate and fix time both degrade as the ephemeris data becomes obsolete. Thus, GPS power costs do not decrease linearly with duty cycle.

Second, the fixing process requires view of three or more satellites. While GPS signals can pass through tree canopies and reflect off of large objects, this

interference can increase the operation time required for the receiver to obtain the necessary information, which costs energy (Moriarty and Epps 2015). If a receiver attempts to make a fix when three or fewer satellites are in view, the attempt will fail, but energy is still expended on decoding the received signal. Furthermore, more satellites provide a more accurate fix, so sampling in open areas is more desirable than sampling in closed or forested areas.

These factors motivate context-sensitive sampling strategies. One approach is to record information about GPS visibility in different locations, and opportunistically sample in open areas. For example, (Lin et al. 2010) maintains a grid map that describes the energy costs and precision results from various locations, and triggers a measurement using whichever sensor that is likely to be the cheapest. GPS visibility can also be inferred from proxy measures such as the amount of sunlight (during the day) and the presence of WiFi signals, which suggest nearby buildings, as in (Paek, Kim, and Govindan 2010).

4.1.3 Uncertainty Supression

Another way to schedule measurements is to model some measure of "uncertainty," and its evolution in time. As the system proceeds, the amount of uncertainty grows. When a GPS measurement is performed, the uncertainty shrinks. Between GPS measurements, low-cost accelerometry measurements can slow the growth of uncertainty in certain ways.

(Jurdak et al. 2010) and (Kjaergaard et al. 2011) employ a simple model, estimating an upper bound on velocity and triggering a measurement when that bound exceeds a threshold. More commonly, uncertainty is taken as the width of a probability distribution. This is a natural measure for Kalman-filter models, such as those used in (Jain and Chang 2004).

4.2 ESCAPE Uncertainty supression strategies

In (Lichtenstein and Elkaim 2019) and (Lichtenstein and Elkaim 2020), we present several strategies for reducing the number of GPS measurements required, while posing a minimized risk of failing to capture unexpected animal behavior. Each strategy is formulated on a different stochastic model of the animal's motion. Each model is then used to build a filter which estimates the animal's position in some way, along with a measure of the uncertainty of that estimate.

The filters can be run in real-time, allowing the tag's on-board controller to trigger GPS measurements only when the uncertainty grows beyond a threshold. In this way, we can throttle costly GPS measurements, while still ensuring that we can record the animal's position with a particular resolution.

The models we present are of varying complexity. Complex models are harder to implement, but may improve GPS sampling efficiency. Also, complex models are at a greater risk of overfitting, so deploying a complex model in the field may produce too many or too few GPS samples. Our goal is to provide a view of the landscape of model complexity, allowing the informed selection of a suitable strategy.

Each of these models utilize a Kalman filter (or can be cast in the form of a Kalman filter), so we give a brief overview of Kalman filters before discussing the models in detail.

4.2.1 The Extended Kalman Filter

A common tool for combining the results of multiple sensors to estimate the state of a system is the Kalman filter. Originally proposed in (Kalman 1960), the Kalman filter is now a foundational approach in modern estimation (Gelb 1974). In the following, we use the notation of (Stengel 2012).

Note that we ignore several elements of more general Kalman filters for simplicity, including only the components that we use in the algorithms we designed. In particular, we ignore any control components (except in rare and ethically dubious cases (Clark 2013), animal control is a rare feature in tags). Also, most of our models have nonlinear dynamics, so we describe general version of the Kalman Filter that is generalized to operate on nonlinear systems, called the Extended Kalman Filter (EKF).

The Kalman filter is an iterative algorithm that takes input from sensors at each step. It maintains an estimate of the system's state in a vector usually denoted as $\bar{\mathbf{x}}$, along with a covariance matrix, $\mathbf{P}$, that estimates uncertainty in $\bar{\mathbf{x}}$. With each new measurement, it iterates, updating $\bar{\mathbf{x}}$ and $\mathbf{P}$. In our application, $\bar{\mathbf{x}}$ usually contains the latitude and longitude displacement of the tag, along with other variables like velocity and heading angle.

To illustrate the evolution of the filter, a section from one test run is shown in Figure 4.1.

This approach is advantageous for tracking for two main reasons. First, a Kalman filter provides a mechanism for combining information from various types of sensors. Secondly, the Kalman filter's covariance matrix is a natural way of measuring uncertainty, which can serve as an input to the GPS uncertainty suppression policy.

EKF Design

To construct an EKF, a dynamics model of the underlying system is required. These take the general form

$$\frac{d}{dt}\mathbf{x} = f(\mathbf{x}) + \mathbf{w}$$

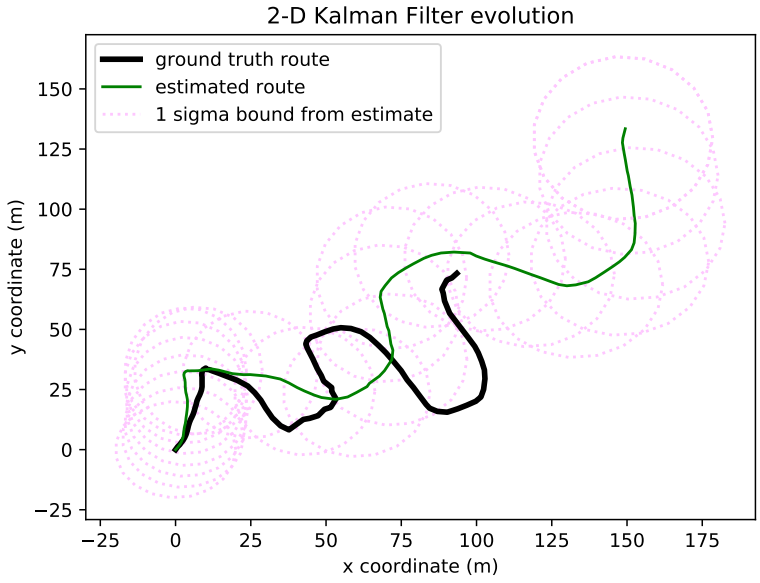

Figure 4.1: The 2-D Kalman filter uses magnetometry information to follow changes in direction. The dotted circles approximately indicate the region within 1-sigma of the estimated location, as measured by the diagonal elements of the covariance matrix.

where $\mathbf{x}$ is the state of the system (distinct from its estimate, $\bar{\mathbf{x}}$), and $\mathbf{w}$ is a Gaussian noise vector with covariance matrix $\mathbf{Q}$. $f()$ is a multi-valued function that outputs a vector with the same size as $\mathbf{x}$. $f()$ can be thought of as representing the predictable component of the dynamics, while $\mathbf{w}$ represents the unpredictable component. The filter designer chooses $f()$ by modeling the physical properties of the system and examining data from previous systems. By defining $f()$, $\mathbf{w}$, and $\mathbf{Q}$, the designer defines the dynamics model of the filter.

The filter also requires a measurement model. This predicts the value $\mathbf{z}$ that a given sensor s would yield if it measured a system in state x These take the general form

$$\mathbf{z}_s = h_s(\mathbf{x}) + \mathbf{n}$$

,

where $\mathbf{n}$ is a Gaussian noise vector with covariance $\mathbf{R}$. $h_s()$ outputs a vector with the same size as $\mathbf{z}_s$ and represents the component of the measured value that can be predicted from $\mathbf{x}$, while $\mathbf{n}$ represents measurement noise. The designer of the filter chooses $h_s()$,$\mathbf{n}$, and $\mathbf{Q}$ for each sensor on the device by modeling the sensors, using a combination of datasheet specifications and calibration information.

There are a few other choices left to the EKF designer. Initial values for the parameters $\bar{\mathbf{x}}$ and $\mathbf{P}$ must be determined, and a method of integrating between measurements must be chosen.

Kalman Filter Update Algorithm

Once online, the EKF updates each time a new measurement arrives from each sensor. For the below, we use the notation $\cdot_{(-)}$ to indicate the value of a variable prior to the update, and $\cdot_{(+)}$ to indicate the value after the update.

The steps to update after receiving a measurement from sensor s are as follows:

First, several Jacobian matrixes are calculated. The Kalman Filter uses linear algebra techniques to perform its error-minimization, so this produces linear local approximations for the non-linear functions $f()$ and $h_s()$.

$$\mathbf{F} = \left.\frac{\partial f()}{\partial \mathbf{x}}\right|_{\bar{\mathbf{x}}_(t)}$$

$$\mathbf{L} = \left.\frac{\partial f()}{\partial \mathbf{w}}\right|_{\bar{\mathbf{x}}(t)}$$

$$\mathbf{H} = \left.\frac{\partial h_s()}{\partial \mathbf{x}}\right|_{\bar{\mathbf{x}}(t)}$$

Next, the values of $\bar{\mathbf{x}}$ and $\mathbf{P}$ are integrated over the time interval since the last update, so they reflect the filter's best estimate of the system's state at the time of measurement according to equation 4.2.1. Since our system receives multiple measurements at a rate of 16 Hz, we opt for a simple linear extrapolation:

$$\mathbf{x}_{(-)} = (t_k - t_{k-1}) \cdot \mathbf{F}(t_{k-1})\bar{\mathbf{x}}(t_{k-1})$$

$$\mathbf{P}_{(-)} = (t_k - t_{k-1}) \cdot [\mathbf{F}(t_{k-1})\mathbf{P}(t_{k-1}) + \mathbf{P}(t_{k-1})\mathbf{F}(t_{k-1}) + \mathbf{L}(t_{k-1})\mathbf{Q}\mathbf{L}(t_{k-1})]$$

Next, the optimal filter gain, $\mathbf{K}$, is calculated. $\mathbf{K}$ can be thought of as a weighting factor for the measurement, determining how much the measurement should affect each element of $\bar{\mathbf{x}}$.

$$\mathbf{K} = \mathbf{P}_{(-)}\mathbf{H}^T \left[\mathbf{H}\mathbf{P}_{(-)}\mathbf{H}^T + \mathbf{R}\right]^{-1}$$

Next, the state vector estimate $\bar{\mathbf{x}}$ is updated to reflect the measurement:

$$\bar{\mathbf{x}}_{(+)} = \bar{\mathbf{x}} + \mathbf{K}\left[\mathbf{z}_s(t) - h(\bar{\mathbf{x}}_{(-)})\right]$$

Next, the covariance estimate is updated. Here, I represents the identity matrix of the same dimension as z.

$$\mathbf{P}_{(+)} = [I - \mathbf{KH}]\,\mathbf{P}_{(-)}$$

In the case of the algorithms that use unit quaternions, the four components of $\bar{\mathbf{x}}$ that describe the quaternion are normalized. At this point, $\bar{\mathbf{x}}_{(-)}$ and $\mathbf{P}_{(-)}$ are discarded, and the algorithm is ready for the next update.

4.2.2 ESCAPE Adaptive Sampling Algorithms

The algorithms here all follow a similar uncertainty suppression strategy. In each, an EKF is constructed such that two elements of $\mathbf{x}$ are the latitude and longitude of the tag's GPS sensor, or else, the displacement of the tag from the last GPS fix. Then, the corresponding diagonal elements of $\mathbf{P}$ added in quadrature serve as a measure of uncertainty in the tag's position.

The algorithm runs the EKF while the GPS is disabled, receiving updates from the IMU. When uncertainty exceeds a threshold, the GPS unit is enabled until a fix is obtained. At that time, $\bar{\mathbf{x}}$ and $\mathbf{P}$ are reset and the GPS is disabled again. The only difference between the algorithms is the Kalman filter at the heart of the algorithm.

Note that at the time of each fix, the Kalman x, y estimate and the ground truth (as revealed by the new fix) have significantly diverged, as can be seen in Figure 4.1. Upon receiving a valid GPS fix, the entire dead reckoning trajectory can be recalculated afterwards to match the new end point, either in real time or during later analysis. This could be accomplished by scaling and rotating the x, y history, as we do in Section 4.3, or by applying a backward-smoothing version of the Kalman filter.

We examined four EKF-based uncertainty suppression algorithms. The "distance-bound" algorithm is the simplest, using the absolute distance from the last GPS measurement as its single state-space parameter, and uses only input from the accelerometer. The "2D" algorithm has a four-dimensional state space, including latitude and longitude, velocity, and heading angle, and incorporating measurements from the accelerometer and gyroscope. The "3D-AM" and "3D-AMG" algorithms have a 14-dimensional state space, including triples for position, linear velocity, and linear acceleration, as well as a quaternion and a triple to record the orientation of the tag and its angular momentum. The former uses the accelerometer and magnetometer, while the latter also uses the gyroscope.

Velocity-bounding model

One very simple model treats the tag as a time-varying random-walk process across the surface of the earth. Several analyses of animal energetics have shown that a quantity called the overall body dynamic acceleration (OBDA) is well correlated with an animal's land velocity ((Qasem et al. 2012), (Williams et al. 2017), (Bryce 2017)). ODBA is obtained using an accelerometer mounted on the trunk of an an animal. As the accelerometer runs, a running sum or similar smoothing filter is applied to each axis, estimating a "static" acceleration vector. Then, this is subtracted from each channel, yielding the dynamic body acceleration (DBA). This vector quantity is then summed to provide a scalar:

$$ODBA(t) = \sum_{i=x,y,z} |A_i(t) - \overline{A_i(t)}|$$

where $\overline{(\cdot)}$ represents the static acceleration. Following (Williams et al. 2017) and (Bryce 2017),we model the ODBA-velocity relationship as linear polynomial:

$$v(ODBA) = \alpha(ODBA) + \beta + n$$

where n is some error, which we treat as Gaussian noise. α and β will be different for each type of animal and mounting arrangement (collar, harness, glue, etc), though are reasonably consistent within species ((Williams et al. 2014)).

To deploy an ODBA-based scheduling algorithm in the field, the ODBA-velocity relationship must be established beforehand. One approach is to perform treadmill experiments, as in (Qasem et al. 2012) or (Bryce, Wilmers, and Williams 2017), in which a captive animal is mounted with a tag and trained to run on a treadmill. An alternate approach, which we use here, is to take the results of previous tracking data to establish an approximate model. See Section 4.2.3 for more detail about this procedure.

Our velocity-bounding model keeps a single state: An estimate of the upper bound of the tag's distance from its last GPS measurement. This is the sole component of $\mathbf{x}$. We call this x. Then, we model x's rate of change as an approximate upper bound on velocity, or v_{lim}:

$$dx(t)/dt = v_{lim}(ODBA(t))$$

Then x serves as the measurement of uncertainty which triggers GPS fixes. [1]

This model has two main advantages: First, it is very simple. Second, it can be implemented with only a 3-axis accelerometer, without requiring a magnetometer or gyrometer. This reduces the power cost of the collar, and the footprint of

[1] This model can be represented by a Kalman Filter by treating $\mathbf{x}$ as a one-dimensional vector which represents the displacement of the tag along some arbitrary axis. Because the ODBA does not provide any information about the direction of the change in x, we set $f(\mathbf{x}) = 0$ and $h_{accel} = 0$, and instead incorporate ODBA in the noise model, $\mathbf{w}(t) = v_{lim}(ODBA(t))$. Then, the lone element of $\mathbf{P}$ is equivalent to x. This mathematically equivalent casting does not match the description of the model in the code used in (Lichtenstein and Elkaim 2019), but is described here for consistency.

the required electronics. It could also be implemented on existing accelerometry collars without altering the hardware.

2D model

The velocity-bounding model assumes all of the estimated velocity of the tag is in a straight line from the last GPS measurement. This is not necessarily the case. One might imagine a puma pacing back and forth, with a significant absolute speed but an average velocity near zero. Such behavior could trigger many GPS measurements, yielding little or no new information.

This is the worst-case power-reduction scenario, but it is probably the best that can be done with only an accelerometer (see (Mizell 2003)). However, by including a magnetometer, a gyrometer, or both, we can gain some knowledge of the tag's orientation, in addition to the animal's land speed. In the duration between GPS measurements, a tag can integrate its accelerometer values to estimate its latitude and longitude.

Given the presence of a magnetometer or gyros, it becomes possible to include estimates of the tag's orientation (attitude or pose), as well as horizontal position. This allows a dead-reckoning estimation between GPS measurements. Our second scheme uses an extended Kalman filter to maintain an estimate of the tag's position and orientation. In this case, the diagonal elements of the Kalman filter's covariance matrix serve as measures of uncertainty.

The 2D EKF uses magnetometry to integrate ODBA measurements with pose estimation. We do not leverage gyroscope measurements, as gyroscopes require significantly more power than magnetometers. The 2-D filter uses a state vector $X = [x, y, v, \theta]$, where x and y are coordinates in a local "flat earth" plane. The origin of this "East-North" frame is re-centered upon each GPS fix so that the

most recent fix is at $x = 0, y = 0$, with the x axis pointing due east at the origin, and the y axis pointing due north at the origin. θ is the heading angle of the tag, or the angle between the x axis and due east as measured in the tag's frame. It updates upon receiving accelerometer and magnetometer measurements. This gives the dynamics equation

$$\begin{bmatrix} \dot{x} \\ y \\ v \\ \theta \end{bmatrix} = \begin{bmatrix} v\cos\theta + w_h \\ v\sin\theta + w_h \\ w_v \\ w_\theta \end{bmatrix}$$

where $v(t)$ is the ODBA-estimated velocity as described Section 4.2.2. w_h describes process noise, interpreted as the motion of the animal that is not predicted by our $v(ODBA)$ model as discussed in Section 4.2.3. Similarly, w_v and w_θ are determined by the maximum horizontal linear and angular acceleration observed during the calibration period.

The accelerometer model is as follows:

$$h_{accel} = ODBA = \frac{v - \beta}{\alpha} + n_{ODBA}$$

where n_{ODBA} is measurement noise, determined during model calibration as described in Section 4.2.3.

The magnetometry model follows two assumptions: First, they assume that the tag's orientation relative to the animal's body is approximately stable, in the sense that the forward-facing axis of the tag continues to point in the general direction of the animal's trajectory. This assumption may be violated if the tag becomes detached or dislodged. Secondly, our magnetometry model assumes that the horizontal component of the Earth's magnetic field, B_{earth}, is approximately

constant over the range covered between GPS fixes. This allows the identification of the horizontal component of the earth's magnetic field, allowing an estimate of heading angle using trigonometry.

$$h_{mag} = \arctan(B_x/B_y) = \theta + n_\theta$$

The "uncertainty" measure in this algorithm is the sum in quadrature of the first two diagonal elements of the covariance matrix, or $\sqrt{\mathbf{P}_{x,x}^2 + \mathbf{P}_{y,y}^2}$.

This model retains much of the simplicity of the first model, but it still relies on a correlational ODBA/velocity relationship. It also relies on the assumption that the tag's z-axis remains more or less vertical during periods of high mobility, as the angle between the magnetic field and gravity is essential for measuring θ.

3D models

The 3D filters attempt to estimate the full position and orientation of the tag in three-dimensional space. The AM model uses only the accelerometer and magnetometer, while the AMG model uses the gyroscope as well.

In the description of the EKF below, we employ two coordinate frames for the tag's body and the frame of the earth. Roughly following the notation of Kim and Golnaraghi 2004, we name our frames "body" and "ground", or b and g respectively. The body frame is the frame of the tag, in which we assume the IMU is fixed. The ground frame is static between GPS fixes, but is re-assigned upon each new fix. It is an "east-north-up" frame, that is, a euclidean frame whose origin is the point at which the most recent GPS fix was acquired. At the origin, x_g points due east, y_g points north, and z_g points up. We wish to estimate the location and attitude of the tag in the ground frame using measurements performed in the body frame.

The rotation between these two frames can be encoded using a unit quaternion. This quaternion is denoted $\mathbf{q} = [q_0, q_1, q_2, q_3]^T$. A rotation matrix, $R_b^g(\mathbf{q})$, can be obtained from this quaternion that allows vectors in the body frame to be rotated into the ground frame (see, for example, Zipfel 2007).

$$R_g^b(\mathbf{q}) = \begin{bmatrix} q_0^2 + q_1^2 - q_2^2 - q_3^2 & 2(q_1q_2 - q_0q_3) & 2(q_0q_2 + q_1q_3) \\ 2(q_1q_2 + q_0q_3) & q_0^2 - q_1^2 + q_2^2 - q_3^2 & 2(q_2q_3 + q_0q_1) \\ 2(q_1q_3 - q_0q_2) & 2(q_0q_1 + q_2q_3) & q_0^2 - q_1^2 - q_2^2 + q_3^2 \end{bmatrix}$$

The 3D-AMG filter has the 16-dimensional state space

$$\mathbf{x} = [\mathbf{x}_g, \mathbf{v}_g, \mathbf{a}_g, \mathbf{q}, \boldsymbol{\omega}_g]^T$$

where $\mathbf{x}_g$, $\mathbf{v}_g$, $\mathbf{a}_g$, and $\boldsymbol{\omega}_g$ are the 3-dimensional vectors in the ground frame describing the position, velocity, acceleration, and rotational velocity of the tag, respectively. $\mathbf{q}$ is the unit quaternion vector described above. The AM filter uses the same state space, but without $\boldsymbol{\omega}_g$, since this set of parameters is only useful only for incorporating gyroscope measurements.[2]

The evolution of this quaternion under ω_g is the product of a matrix $\boldsymbol{\Omega}$, which describes the angular momentum, and the quaternion:

$$\dot{\mathbf{q}} = \frac{1}{2}\boldsymbol{\Omega}\mathbf{q} = 1/2 \begin{bmatrix} 0 & -\omega_x & -\omega_y & -\omega_z \\ \omega_x & 0 & -\omega_z & \omega_y \\ \omega_y & \omega_z & 0 & -\omega_x \\ \omega_z & -\omega_y & \omega_x & 0 \end{bmatrix} \mathbf{q}$$

[2]More formally, the rows of $\mathbf{K}$ that correspond to $\boldsymbol{\omega}_g$ are zero for the accelerometer and magnetometer update steps.

This gives a dynamics equation

$$\begin{bmatrix} \dot{\mathbf{x}}_g \\ \mathbf{v}_g \\ \mathbf{a}_g \\ \mathbf{q} \\ \boldsymbol{\omega}_g \end{bmatrix} = \begin{bmatrix} \mathbf{v}_g \\ \mathbf{a}_g - \mathbf{v}_g \cdot \alpha \\ 0 \\ \frac{1}{2} \cdot \boldsymbol{\Omega} \cdot \mathbf{q} \\ 0 \end{bmatrix} + \begin{bmatrix} \mathbf{w}_x \\ \mathbf{w}_v \\ \mathbf{w}_a \\ \mathbf{w}_q \\ \mathbf{w}_w \end{bmatrix}$$

Here, w_x, w_v, w_a, and w_ω are 3×1 vectors that describe process noise for the corresponding state vector elements. For simplicity, we use an isotropic model, so each of these is simply one scalar value repeated. The values of these parameters were obtained by inspecting ground truth data from trial runs. $\mathbf{w}_q$ are the process noises for the state space parameters. α is a damping factor on v. Since no sensor (besides the occasional GPS) observes velocity, this factor is necessary to prevent the estimated values in x from drifting while the tag is stationary. These values were obtained through trial and error on simulations using trial run data.

For the AM filter, the last row of the dynamics equation vector is removed.

In the 3D filters, acceleration measurements are modeled as

$$z_{accel} = \begin{bmatrix} a_{b,x} \\ a_{b,y} \\ a_{b,z} \end{bmatrix} = R(q_g^b) \cdot \left(a_g + \begin{bmatrix} 0 \\ 0 \\ g \end{bmatrix} \right) + n_{accel}$$

where $a_{b,i}$ represent calibrated accelerometry measurements by the IMU on the i axis in the body frame, and g is acceleration due to gravity.

Magnetometry measurements are modeled as

$$z_{mag} = \begin{bmatrix} B_{b,x} \\ B_{b,y} \\ B_{b,z} \end{bmatrix} = R(q_g^b) \cdot B_g + n_{mag}$$

where B_g is the magnetic field of the earth near the location of the collar.

Gyroscope measurements are modeled as

$$z_{gyro} = \begin{bmatrix} \omega_{b,x} \\ \omega_{b,y} \\ \omega_{b,z} \end{bmatrix} = R(q_g^b) \cdot \omega_g$$

The gyroscope was assumed to have negligible drift over the course of the experimental run, but in future long-term versions this measurement should contain a term to correct for drift.

The measurement noises for each of the 9 axes in the IMU sensor are assumed to be uncorrelated.

The 3D approaches are significantly more complicated, presenting various implementation and debugging challenges. The advantage to such an approach is that it allows all IMU sensors to be fused into a state estimate in a consistent way. Additionally, if successful, the 3D model reconstructs the route of the tag with a high degree of detail.

4.2.3 Experiment Design

The algorithms were tested by attaching a device to a human using a chest harness and performing several runs. During each run, a second device ran a GPS unit continuously to establish ground truth. An initial run was performed

to provide data to establish model parameters for process noise.

The device used to run the algorithm was an LG G3 VS985 mobile phone. This chosen because it contained the sensor hardware with which an animal tag might be equipped, along with a convenient toolchain. The device has been rooted, allowing the GPS module to be fully power-cycled, and allowing any A-GPS features to be disabled. The algorithms are run using an Android service, which also continuously records a variety of data including the measurements of all sensors, the state vectors and covariences of each algorithm, and the cumulative GPS uptime.

Sensors in the VS985 were calibrated using an hour of data from the device in static positions in several different orientations. This data was used to establish bias and scaling for each sensor.

These runs comprised of a fixed sequence of jogging, walking, sprinting, and sitting along a predetermined route. The periods of activity were alternated at fixed landmarks, and the route included a variety of terrains and curvatures.

After each run, an estimated route was reconstructed by dividing the record of $\hat{x}_g$ into intervals between GPS fixes. Each interval was then translated and rotated so that its start- and end-points aligned with the measured GPS fixes.

Establishing model constant parameters

An initial run was performed to provide data to establish model parameters.

The ODBA-velocity relationship used in the distance-bound model and the 2D model was established by dividing the run into intervals between GPS measurements. In each interval, an average ODBA was calculated, and paired with the GPS-velocity of that interval (that is, the absolute horizontal distance between GPS the two measurements divided by the duration of the interval). These ODBA-vs-velocity pairs were then binned by average ODBA. For each bin, the

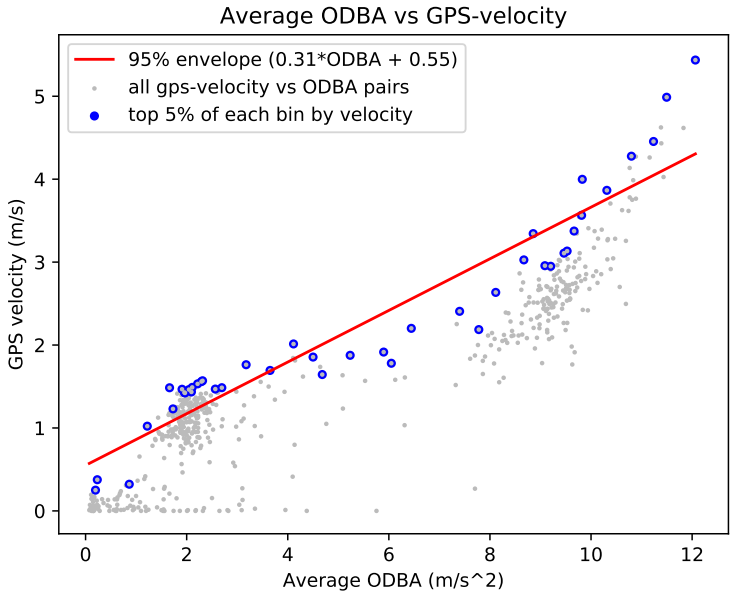

Figure 4.2: ODBA vs GPS veloicty. This diagram is taken from an analysis of data used in (Wang et al. 2015)

5% of pairs with the largest GPS velocity were added to the set of worst-case pairs.[3] A linear regression was employed for this worst-case set to determine the α and β parameters for our $v(ODBA)$ model. The residual standard error of this regression becomes n_{ODBA}. This procedure is illustrated in 4.2.

4.3 Results

We compared the results of test runs using the distance-bound, 2D, 3D-AM, and 3D-AMG algorithms, along with the results from a fixed-period schedule. The reconstructed routes for each algorithm can be seen in 4.3

The GPS uptime of each algorithm is shown in Fig. 4.4. Both the AM and AMG algorithms produced higher cumulative uptime, but these uptimes were concentrated in particular areas.

[3]We chose to use the most extreme intervals in order to produce a conservative model.

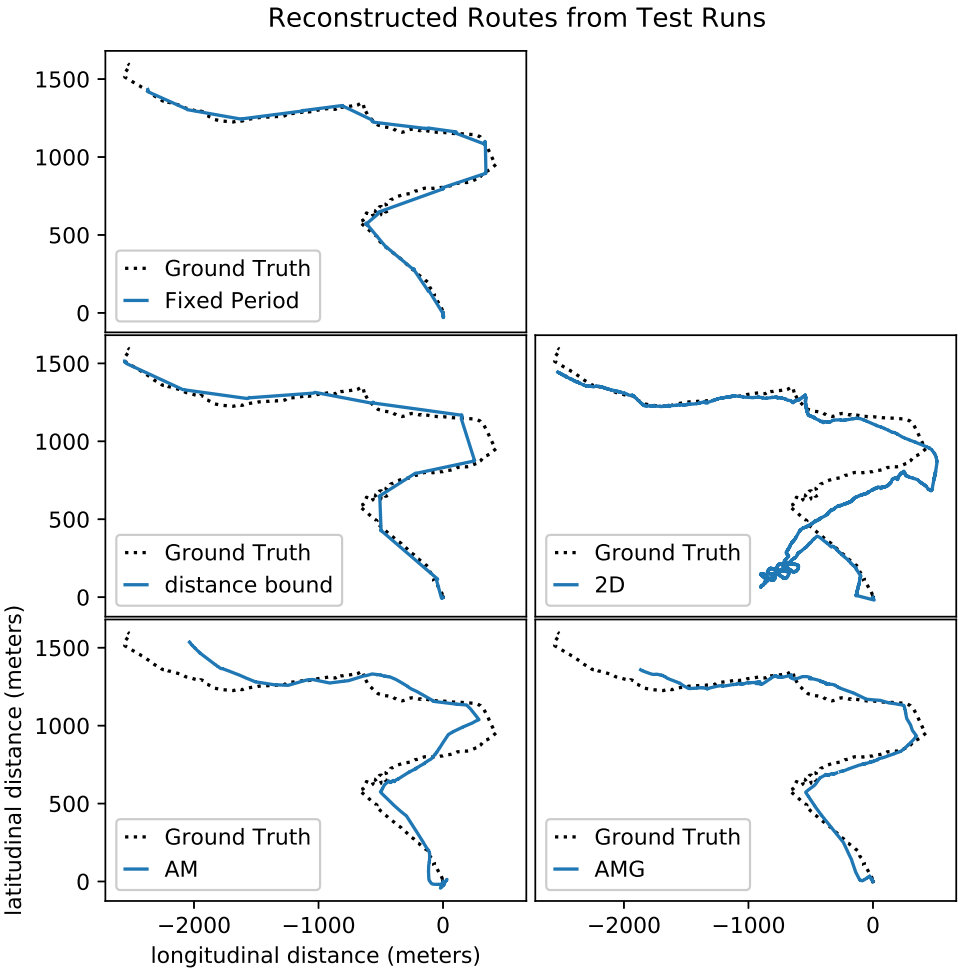

Figure 4.3: Reconstructed and ground-truth routes for each trial run. Distances are measured with respect to starting point.

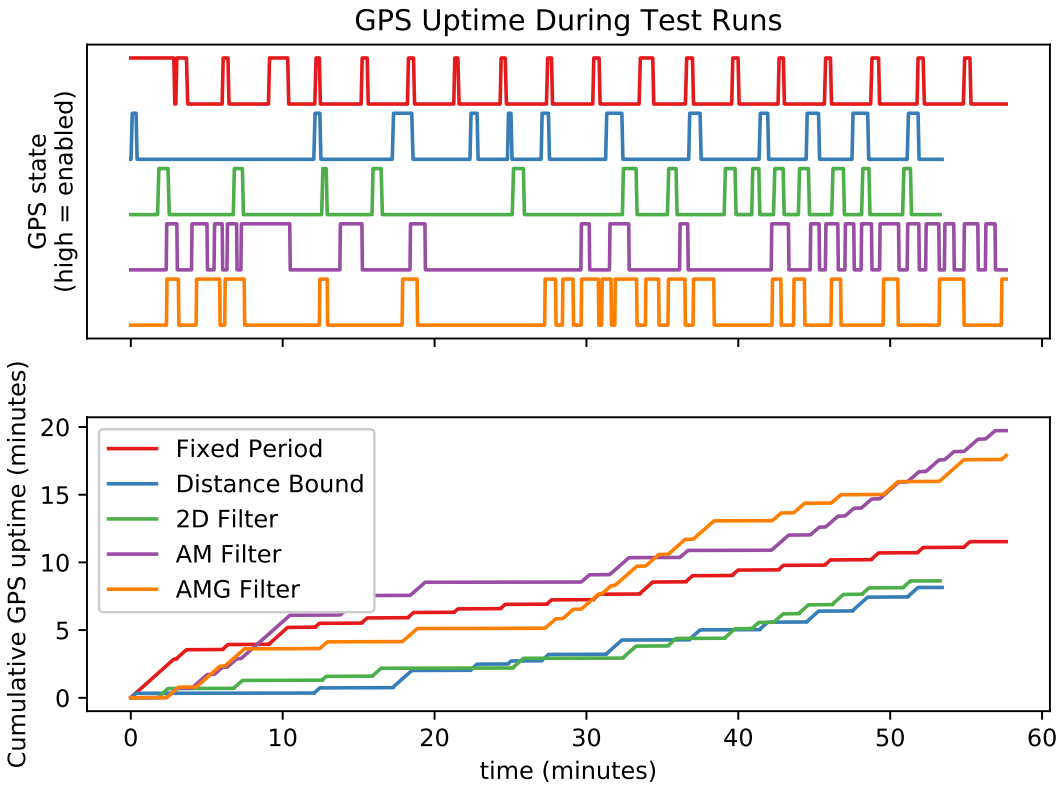

Figure 4.4: GPS uptime records during each test run.

Each run was evaluated for accuracy by a time-averaged error. For each second, the distance between the reconstructed-route estimate for x and the ground truth was computed. Fig. 4.5 shows the distribution of these errors. While the AM and AMG filters produce extreme errors, these are more concentrated at small error regions.

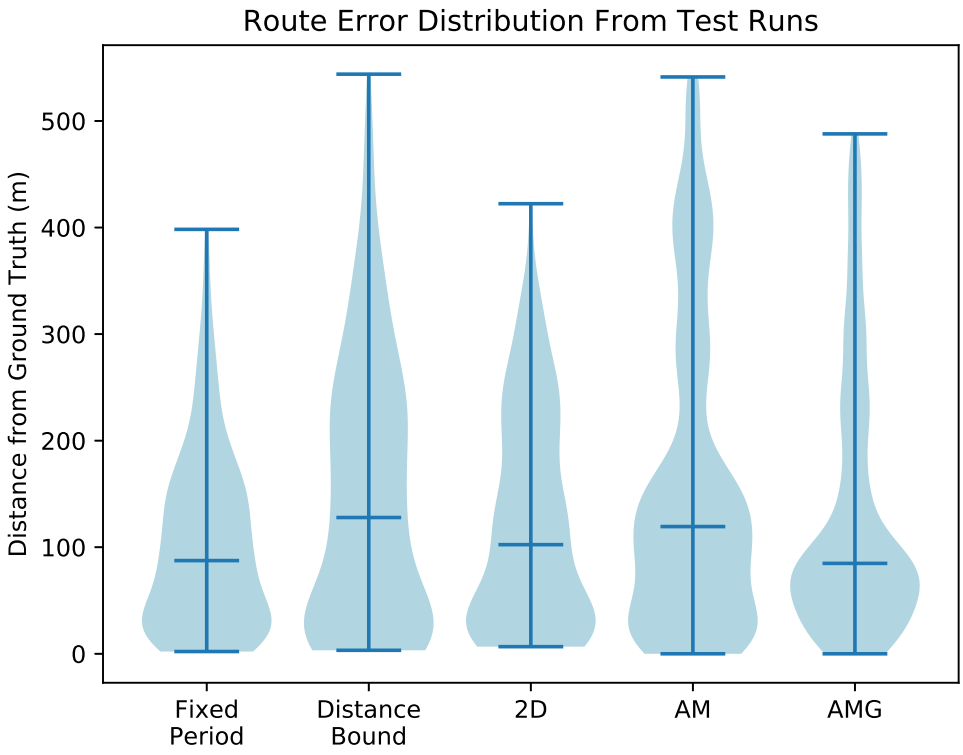

Figure 4.5: Violin plots for route error distribution across GPS scheduling algorithms. Horizontal ticks represent the median of each distribution.

By inspection, the reconstructed routes generally seem to follow the ground truth routes. However, in some segments, the filter demonstrates extreme behavior and diverges strongly from the route.

4.4 Discussion

The algorithms in this paper were built on the principle of a general dynamics model that assumed as little as possible about the orientation of the tag or the behavior of the animal. This seems to have a severe impact on the ability of the Kalman filter to perform tracking. A more specific dynamics model may be able to recover the ability to accurately estimate routes.

It is possible that these principles would preserve fidelity in the case of a tag that has been moved or dislodged by animal activity. However, our experimental test did not account for this possibility. Future work should test this approach in situations where the orientation of the IMU is altered during a run.

While no individual route exhibited both high tracking fidelity and conservative GPS uptime performance across the entire route, most sections of the route were efficiently tracked by at least one algorithm. Also, the AM and AMG filters each exhibited periods of high power consumption. A multi-modal filter might be able to detect if a particular filter is failing, and switch instead to a power policy guided by a more appropriate filter.

We also should note several respects in which these tests may not predict in-field performance. A chest-mounted device on a human may exhibit some structure that a tag mounted on an animal's collar or shell would not. For example, collars can rotate about the neck of the subject animal, and each animal has different patterns of motion which may effect the evolution of these algorithms. Ultimately, testing on an animal subject is required for a full evaluation of the efficacy of this approach.

Additionally, our tests do not reflect a natural distribution of animal activity. Sleeping and walking are usually more common than running, but these behaviors are undersampled by our testing procedure. A more exact test would capture at

least a full day of behavior, thus allowing each behavior to influence the algorithm according to its share of overall behavior.

Chapter 5

Conclusion

5.1 Conclusion

We have explored several routes for expanding the life of animal tags. In some cases, these findings illuminate potential for viable power-reduction strategies in real-world tagging applications, and in other cases suggest some strategies are likely to be unfeasible. We now review these findings.

Scavenging solar power seems unambiguously promising. Results reported by (Wilson et al. 2013), (Jurdak et al. 2013a) demonstrate in real-world field deployents that the energy these tags scavenge is signficant. Though its yields are intermittent, unpredictable, and potentially short-lived, the density of solar radiation makes it plausible that the limited conditions of solar scavenging might make up for the weight and volume costs.

We also performed a theoretical examination of the upper limits of thermal energy scavenging. Our analysis suggests that thermal energy scavenging could be a signficant and useful source of energy for a tag on some animals, but it is not clear if real-world thermal scavenging designs could deliver anywhere near the theoretical upper bound estimate that we find. More research is needed, and this

line of development is probably best advanced in human wearable technology for the time being.

For kinetic scavenging, we conduct a novel analysis of oscillating kinetic harvesters, supplemented with experimental tests on a commonly proposed kinetic harvester. Both lines of evidence point to the same conclusion: Kinetic harvesters are incapable of offsetting their own weight in batteries given present tag technology. If the energy consumption of tag payloads were to drop several orders of magnitude, kinetic harvesters could become viable, but until such time, they are best replaced by batteries.

We examined in depth an adaptive GPS scheduling technique, developing and testing four versions of an EKF-based uncertainty suppression algorithm. These algorithms are presented as alternatives to other adaptive sampling techniques whose models are less explicit and whose assumptions are more arbitrary. These algorithms succeed in showing that this approach can mediate between over-measuring, which costs energy, and under-measuring, which costs accuracy. The simpler algorithms, the 2D and distance-bound algorithm, reduced GPS uptime when compared with the commonly deployed fixed sampling interval, but the reconstructed route after the test deviated more from ground truth. The 3D-AMG model improved accuracy in some measure [1], but increased uptime. And the 3D-AM model underperformed a fixed interval strategy in every respect.

When computational and implementation costs of these algorithms are considered, it is unclear if any of the algorithms developed in this work are a clear victory for the EKF-based uncertainty suppression approach. This may reflect a fundamental challenge in modeling a living animal with an EKF. The EKF, requires some measure of predictability in its underlying system, and animals are by nature somewhat unpredictable. It is possible that the 2D algorithm performed

[1] specifically, the mean route error over time

the best because it represents the best model that can be made of a land animal with the measurement energy available. It is also possible that a 3D estimator is possible, but yet to be created. As discussed in Section 4.4, techniques such as the unscented Kalman Filter or a particle filter approach may be able to avoid some of the pitfalls our 3D models encountered.

While this work reveals few promising pathways for advancement that were not clear prior to its undertaking, the work does provide useful evidence against the potential in some approaches.

Chapter 6

References

Bibliography

Adoram-Kershner, Lauren et al. (2017). "Modeling and Testing Solar Power for Globally Migrating Submarine Systems". In: *OCEANS–Anchorage, 2017*. IEEE, pp. 1–9.

Aktakka, Ethem Erkan, Hanseup Kim, and Khalil Najafi (2011). "Energy Scavenging from Insect Flight". In: *Journal of Micromechanics and Microengineering* 21.9, p. 095016.

Andersen, David E. (1994). "Longevity of Solar-Powered Radio Transmitters on Buteonine Hawks in Eastern Colorado (Longevidad de Radiotransmisores Con Baterías Solares Colocados En Buteos Del Este de Colorado)". In: *Journal of Field Ornithology*, pp. 122–132.

Antoine-Santoni, Thierry et al. (Sept. 3, 2018). "AMBLoRa: A Wireless Tracking and Sensor System Using Long Range Communication to Monitor Animal Behavior". In:

Basset, P. et al. (2009). "A Batch-Fabricated and Electret-Free Silicon Electrostatic Vibration Energy Harvester". In: *Journal of Micromechanics and Microengineering* 19.11, p. 115025. ISSN: 0960-1317. DOI: 10.1088/0960-1317/19/11/115025.

Bauer, Christine (2013). "On the (In-)Accuracy of GPS Measures of Smartphones: A Study of Running Tracking Applications". In: *Proceedings of International Conference on Advances in Mobile Computing & Multimedia*. MoMM '13. New York, NY, USA: ACM, 335:335–335:341. ISBN: 978-1-4503-2106-8. DOI: 10.1145/2536853.2536893.

Bhandari, C. M. and David M. Rowe (1995). "CRC Handbook of Thermoelectrics". In: *CRC Press, Boca Raton, FL*, p. 49.

Bhattacharya, Amiya and Sajal K. Das (Mar. 1, 2002). "LeZi-Update: An Information-Theoretic Framework for Personal Mobility Tracking in PCS Networks". In: *Wireless Networks* 8.2, pp. 121–135. ISSN: 1572-8196. DOI: 10.1023/A:1013759724438.

Bonfiglio, Annalisa and Danilo Emilio de Rossi, eds. (2011). *Wearable Monitoring Systems*. New York, N. Y: Springer. 296 pp. ISBN: 978-1-4419-7383-2 978-1-4419-7384-9.

Bowers, Benjamin J and David P Arnold (2008). "Spherical Magnetic Generators for Bio-Motional Energy Harvesting". In: p. 4.

Brown, Danielle D. et al. (Mar. 1, 2012). "Accelerometer-Informed GPS Telemetry: Reducing the Trade-off between Resolution and Longevity". In: *Wildlife Society Bulletin* 36.1, pp. 139–146. ISSN: 1938-5463. DOI: 10.1002/wsb.111.

Bryce, Caleb M. (2017). "Movement Energetics across Landscapes: A Canid Case Study". UC Santa Cruz. URL: https://escholarship.org/uc/item/13q463p7 (visited on 10/31/2018).

Bryce, Caleb M., Christopher C. Wilmers, and Terrie M. Williams (Aug. 17, 2017). "Energetics and Evasion Dynamics of Large Predators and Prey: Pumas *vs.* Hounds". In: *PeerJ* 5, e3701. ISSN: 2167-8359. DOI: 10.7717/peerj.3701.

Burger Jr, Loren W. et al. (1991). "Radio Transmitters Bias Estimation of Movements and Survival". In: *The Journal of wildlife management*, pp. 693–697.

Carreon-Bautista, S. et al. (Oct. 2014). "Boost Converter With Dynamic Input Impedance Matching for Energy Harvesting With Multi-Array Thermoelectric Generators". In: *IEEE Transactions on Industrial Electronics* 61.10, pp. 5345–5353. ISSN: 0278-0046. DOI: 10.1109/TIE.2014.2300035.

Cepnik, Clemens, Roland Lausecker, and Ulrike Wallrabe (Apr. 29, 2013). "Review on Electrodynamic Energy Harvesters—A Classification Approach". In: *Micromachines* 4.2, pp. 168–196. DOI: 10.3390/mi4020168.

Choi, Dong-Hoon et al. (2011). "Liquid-Based Electrostatic Energy Harvester with High Sensitivity to Human Physical Motion". In: *Smart Materials and Structures* 20.12, p. 125012. ISSN: 0964-1726. DOI: 10.1088/0964-1726/20/12/125012.

Church, K. E. (1980). "Expanded Radio Tracking Potential in Wildlife Investigations with the Use of Solar Transmitters". In: *A Handbook on Biotelemetry and Radio Tracking*. Elsevier, pp. 247–250.

Churchill, David L. et al. (July 22, 2003). "Strain Energy Harvesting for Wireless Sensor Networks". In: *Smart Structures and Materials 2003: Smart Electronics, MEMS, BioMEMS, and Nanotechnology*. Smart Structures and Materials 2003: Smart Electronics, MEMS, BioMEMS, and Nanotechnology. Vol. 5055. International Society for Optics and Photonics, pp. 319–328. DOI: 10.1117/12.483591.

Clark, Liat (June 10, 2013). "In Defence of the Cockroach: RoboRoach Kickstarter Ignores Ethics". In: *Wired UK*. ISSN: 1357-0978. URL: https://www.wired.co.uk/article/roboroach-kickstarter (visited on 11/26/2020).

Cochran, William W. and Rexford D. Lord (1963). "A Radio-Tracking System for Wild Animals". In: *The Journal of Wildlife Management* 27.1, pp. 9–24. ISSN: 0022-541X. DOI: 10.2307/3797775. JSTOR: 3797775.

D'Eon, Robert G. and Donna Delparte (2005). "Effects of Radio-Collar Position and Orientation on GPS Radio-Collar Performance, and the Implications of PDOP in Data Screening". In: *Journal of Applied Ecology* 42.2, pp. 383–388.

Donelan, J. M. et al. (Feb. 8, 2008). "Biomechanical Energy Harvesting: Generating Electricity During Walking with Minimal User Effort". In: *Science* 319.5864, pp. 807–810. ISSN: 0036-8075, 1095-9203. DOI: 10.1126/science.1149860. pmid: 18258914.

Dunne, Maxwell James (2014). "Design and Implementation of a Power-Aware Dynamically Sampling Wildlife Collar". UC Santa Cruz. URL: https://escholarship.org/uc/item/2qn232kw (visited on 10/03/2018).

Freunek, Michael et al. (July 1, 2009). "New Physical Model for Thermoelectric Generators". In: *Journal of Electronic Materials* 38.7, pp. 1214–1220. ISSN: 1543-186X. DOI: 10.1007/s11664-009-0665-y.

Gelb, Arthur (1974). *Applied Optimal Estimation*. Red. by Analytic Sciences Corporation. MIT Press. 388 pp. ISBN: 978-0-262-57048-0. Google Books: KlFrn8lpPP0C.

Gorlatova, Maria et al. (2014). "Movers and Shakers: Kinetic Energy Harvesting for the Internet of Things". In: *The 2014 ACM International Conference on Measurement and Modeling of Computer Systems*. SIGMETRICS '14. New York, NY, USA: ACM, pp. 407–419. ISBN: 978-1-4503-2789-3. DOI: 10.1145/2591971.2591986.

Goto, H., T. Sugiura, and T. Kazui (1998). "Feasibility of the Automatic Generating System (AGS) for Quartz Watches as a Leadless Pacemaker Power Source: A Preliminary Report". In: *Engineering in Medicine and Biology Society, 1998. Proceedings of the 20th Annual International Conference of the IEEE*. IEEE, pp. 417–419.

Granstrom, Jonathan et al. (2007). "Energy Harvesting from a Backpack Instrumented with Piezoelectric Shoulder Straps". In: *Smart Materials and Structures* 16.5, p. 1810. ISSN: 0964-1726. DOI: 10.1088/0964-1726/16/5/036.

Halámková, Lenka et al. (Mar. 8, 2012). *Implanted Biofuel Cell Operating in a Living Snail*. DOI: 10.1021/ja211714w.

Halim, Miah A. and Jae Y. Park (Mar. 3, 2014). "A Non-Resonant, Frequency up-Converted Electromagnetic Energy Harvester from Human-Body-Induced Vibration for Hand-Held Smart System Applications". In: *Journal of Applied Physics* 115.9, p. 094901. ISSN: 0021-8979. DOI: 10.1063/1.4867216.

Hoang, Duc Chinh et al. (Nov. 2, 2009). "Thermal Energy Harvesting From Human Warmth for Wireless Body Area Network in Medical Healthcare System". In: *The Eighth International Conference on Power Electronics and Drive Systems (PEDS 2009)*. URL: http://ir.lib.ntust.edu.tw/handle/987654321/14432 (visited on 10/10/2018).

Hubel, Tatjana Y. et al. (Mar. 29, 2016). "Additive Opportunistic Capture Explains Group Hunting Benefits in African Wild Dogs". In: *Nature Communications* 7, p. 11033. ISSN: 2041-1723. DOI: 10.1038/ncomms11033.

Jain, Ankur and Edward Y. Chang (2004). "Adaptive Sampling for Sensor Networks". In: *Proceeedings of the 1st International Workshop on Data Management for Sensor Networks: In Conjunction with VLDB 2004*. ACM, pp. 10–16.

Jain, Vishwas Raj et al. (2008). "wildCENSE: GPS Based Animal Tracking System". In: *Intelligent Sensors, Sensor Networks and Information Processing, 2008. ISSNIP 2008. International Conference On*. IEEE, pp. 617–622.

Janis, Michael W., Joseph D. Clark, and Craig S. Johnson (1999). "Predicting Mountain Lion Activity Using Radiocollars Equipped with Mercury Tip-Sensors". In: *Wildlife Society Bulletin (1973-2006)* 27.1, pp. 19–24. ISSN: 0091-7648. JSTOR: 3783934.

Juang, Philo et al. (2002). "Energy-Efficient Computing for Wildlife Tracking: Design Tradeoffs and Early Experiences with ZebraNet". In: *ACM SIGARCH Computer Architecture News* 30.5, pp. 96–107.

Jurdak, Raja et al. (2010). "Adaptive GPS Duty Cycling and Radio Ranging for Energy-Efficient Localization". In: *Proceedings of the 8th ACM Conference on Embedded Networked Sensor Systems*. SenSys '10. New York, NY, USA: ACM, pp. 57–70. ISBN: 978-1-4503-0344-6. DOI: 10.1145/1869983.1869990.

Jurdak, Raja et al. (2013a). "Camazotz: Multimodal Activity-Based GPS Sampling". In: *Proceedings of the 12th International Conference on Information Processing in Sensor Networks*. IPSN '13. New York, NY, USA: ACM, pp. 67–78. ISBN: 978-1-4503-1959-1. DOI: 10.1145/2461381.2461393.

Jurdak, Raja et al. (2013b). "Energy-Efficient Localization: GPS Duty Cycling with Radio Ranging". In: *ACM Transactions on Sensor Networks (TOSN)* 9.2, p. 23.

Kalman, R. E. (Mar. 1, 1960). "A New Approach to Linear Filtering and Prediction Problems". In: *Journal of Basic Engineering* 82.1, pp. 35–45. ISSN: 0098-2202. DOI: 10.1115/1.3662552.

Kenward, R. E. (2001). *A Manual for Wildlife Tracking*. London, UK: Academic Press.

Kiely, J. J. et al. (Dec. 1991). "Low Cost Miniature Thermoelectric Generator". In: *Electronics Letters* 27.25, pp. 2332–2334. ISSN: 0013-5194. DOI: 10.1049/el:19911444.

Kim, A. and M. F. Golnaraghi (Apr. 2004). "A Quaternion-Based Orientation Estimation Algorithm Using an Inertial Measurement Unit". In: *PLANS 2004. Position Location and Navigation Symposium (IEEE Cat. No.04CH37556)*. PLANS 2004. Position Location and Navigation Symposium (IEEE Cat. No.04CH37556), pp. 268–272. DOI: 10.1109/PLANS.2004.1309003.

Kim, Min-Ki et al. (2014). "Wearable Thermoelectric Generator for Harvesting Human Body Heat Energy". In: *Smart Materials and Structures* 23.10, p. 105002. ISSN: 0964-1726. DOI: 10.1088/0964-1726/23/10/105002.

Kjaergaard, Mikkel Baun et al. (2011). "Energy-Efficient Trajectory Tracking for Mobile Devices". In: *Proceedings of the 9th International Conference on Mobile Systems, Applications, and Services*. ACM, pp. 307–320.

Kulah, Haluk and Khalil Najafi (2004). "An Electromagnetic Micro Power Generator for Low-Frequency Environmental Vibrations". In: *Micro Electro Mechanical Systems, 2004. 17th IEEE International Conference on.(MEMS)*. IEEE, pp. 237–240.

Laundré, John W. (2005). "Puma Energetics: A Recalculation". In: *The Journal of Wildlife Management* 69.2, pp. 723–732. ISSN: 0022-541X. JSTOR: 3803743.

Leonov, V. (June 2013). "Thermoelectric Energy Harvesting of Human Body Heat for Wearable Sensors". In: *IEEE Sensors Journal* 13.6, pp. 2284–2291. ISSN: 1530-437X. DOI: 10.1109/JSEN.2013.2252526.

Leonov, V. and P. Fiorini (2007). "Thermal Matching of a Thermoelectric Energy Scavenger with the Ambience". In: *Proceedings of the European Conference on Thermoelectrics*, pp. 129–133.

Leonov, Vladimir (Apr. 2011). "Simulation of Maximum Power in the Wearable Thermoelectric Generator with a Small Thermopile". In: *Microsystem Technologies* 17.4, pp. 495–504. ISSN: 0946-7076, 1432-1858. DOI: 10.1007/s00542-011-1262-6.

Li, X et al. (Dec. 4, 2013). "Non-Resonant Electromagnetic Energy Harvester for Car-Key Applications". In: *Journal of Physics: Conference Series* 476, p. 012096. ISSN: 1742-6588, 1742-6596. DOI: 10.1088/1742-6596/476/1/012096.

Lichtenstein, Max and Gabriel Elkaim (Apr. 23, 2020). "Efficient GPS Scheduling in Wildlife Tags Using an Extended Kalman Filter-Based Uncertainty Suppression Strategy". In: 2020 IEEE/ION Position, Location and Navigation Symposium (PLANS), pp. 1472–1475. URL: http://www.ion.org/publications/abstract.cfm?jp=p&articleID=17422 (visited on 11/25/2020).

Lichtenstein, Maxwell and Gabriel Hugh Elkaim (Oct. 11, 2019). "Filtering and Sensor Augmentation for GPS Measurement Reduction in Wildlife Tags". In: 32nd International Technical Meeting of the Satellite Division of The Institute of Navigation (ION GNSS+ 2019). Miami, Florida, pp. 1356–1363. DOI: 10.33012/2019.16875.

Lin, Kaisen et al. (2010). "Energy-Accuracy Trade-off for Continuous Mobile Device Location". In: *Proceedings of the 8th International Conference on Mobile Systems, Applications, and Services*. ACM, pp. 285–298.

Lincoln, Frederick C. (1921). "The History and Purposes of Bird Banding". In: *The Auk* 38.2, pp. 217–228. ISSN: 0004-8038. DOI: 10.2307/4073884. JSTOR: 4073884.

Lu, X. et al. (2015). "Wireless Networks With RF Energy Harvesting: A Contemporary Survey". In: *IEEE Communications Surveys Tutorials* 17.2, pp. 757–789. ISSN: 1553-877X. DOI: 10.1109/COMST.2014.2368999.

Mac Kenzie, C. M. (1967). "Solar Power Systems for Satellites in Near-Earth Orbits". In:

MacCurdy, Robert et al. (2008). "A Methodology for Applying Energy Harvesting to Extend Wildlife Tag Lifetime". In: *Volume 8: Energy Systems: Analysis, Thermodynamics and Sustainability; Sustainable Products and Processes*. ASME 2008 International Mechanical Engineering Congress and Exposition. Boston, Massachusetts, USA: ASME, pp. 121–130. ISBN: 978-0-7918-4869-2. DOI: 10.1115/IMECE2008-68082.

MacVittie, Kevin et al. (2013). "From "Cyborg" Lobsters to a Pacemaker Powered by Implantable Biofuel Cells". In: *Energy & Environmental Science* 6.1, pp. 81–86. DOI: 10.1039/C2EE23209J.

Marks, Jeffrey S. and Victoria Saab Marks (1987). "Influence of Radio Collars on Survival of Sharp-Tailed Grouse". In: *The Journal of wildlife management*, pp. 468–471.

Martiskainen, Paula et al. (June 1, 2009). "Cow Behaviour Pattern Recognition Using a Three-Dimensional Accelerometer and Support Vector Machines". In: *Applied Animal Behaviour Science* 119.1, pp. 32–38. ISSN: 0168-1591. DOI: 10.1016/j.applanim.2009.03.005.

McNab, Brian K (2000). "The Standard Energetics of Mammalian Carnivores: Felidae and Hyaenidae". In: 78, p. 13.

Mech, L. David and Shannon M. Barber (2002). *A Critique of Wildlife Radio-Tracking and Its Use in National Parks*. Northern Prairie Wildlife Research Center.

Mitcheson, P D et al. (Sept. 1, 2007). "Performance Limits of the Three MEMS Inertial Energy Generator Transduction Types". In: *Journal of Micromechanics and Microengineering* 17.9, S211–S216. ISSN: 0960-1317, 1361-6439. DOI: 10.1088/0960-1317/17/9/S01.

Mitcheson, P. D. et al. (Sept. 2008). "Energy Harvesting From Human and Machine Motion for Wireless Electronic Devices". In: *Proceedings of the IEEE* 96.9, pp. 1457–1486. ISSN: 0018-9219. DOI: 10.1109/JPROC.2008.927494.

Mizell, D. (2003). "Using Gravity to Estimate Accelerometer Orientation". In: *Seventh IEEE International Symposium on Wearable Computers, 2003. Proceedings.* Seventh IEEE International Symposium on Wearable Computers, 2003. White Plains, NY, USA: IEEE, pp. 252–253. ISBN: 978-0-7695-2034-6. DOI: 10.1109/ISWC.2003.1241424.

Morales, Juan Manuel et al. (2004). "Extracting More out of Relocation Data: Building Movement Models as Mixtures of Random Walks". In: *Ecology* 85.9, pp. 2436–2445.

Moriarty, Katie M. and Clinton W. Epps (June 1, 2015). "Retained Satellite Information Influences Performance of GPS Devices in a Forested Ecosystem". In: *Wildlife Society Bulletin* 39.2, pp. 349–357. ISSN: 1938-5463. DOI: 10.1002/wsb.524.

Paek, Jeongyeup, Joongheon Kim, and Ramesh Govindan (2010). "Energy-Efficient Rate-Adaptive GPS-Based Positioning for Smartphones". In: *Proceedings of*

the 8th International Conference on Mobile Systems, Applications, and Services. ACM, pp. 299–314.

Patton, David R., David W. Beaty, and Ronald H. Smith (1973). "Solar Panels: An Energy Source for Radio Transmitters on Wildlife". In: *The Journal of Wildlife Management* 37.2, pp. 236–238. ISSN: 0022-541X. DOI: 10.2307/3798910. JSTOR: 3798910.

Piñuela, M., P. D. Mitcheson, and S. Lucyszyn (July 2013). "Ambient RF Energy Harvesting in Urban and Semi-Urban Environments". In: *IEEE Transactions on Microwave Theory and Techniques* 61.7, pp. 2715–2726. ISSN: 0018-9480. DOI: 10.1109/TMTT.2013.2262687.

Pillatsch, P, E M Yeatman, and A S Holmes (Nov. 1, 2012). "A Scalable Piezoelectric Impulse-Excited Energy Harvester for Human Body Excitation". In: *Smart Materials and Structures* 21.11, p. 115018. ISSN: 0964-1726, 1361-665X. DOI: 10.1088/0964-1726/21/11/115018.

Pillatsch, Pit, Eric M. Yeatman, and Andrew S. Holmes (2014). "A Piezoelectric Frequency Up-Converting Energy Harvester with Rotating Proof Mass for Human Body Applications". In: *Sensors and Actuators A: Physical* 206, pp. 178–185.

Qasem, Lama et al. (Feb. 17, 2012). "Tri-Axial Dynamic Acceleration as a Proxy for Animal Energy Expenditure; Should We Be Summing Values or Calculating the Vector?" In: *PLOS ONE* 7.2, e31187. ISSN: 1932-6203. DOI: 10.1371/journal.pone.0031187.

Rodgers, Arthur R. (2001). "Tracking Animals with GPS: The First 10 Years". In: *Tracking Animals with GPS. An International Conference*, pp. 1–10.

Romero, E., R. O. Warrington, and M. R. Neuman (2009). "Energy Scavenging Sources for Biomedical Sensors". In: *Physiological measurement* 30.9, R35.

Roundy, Shad, Paul Kenneth Wright, and Jan M. Rabaey (2003). "Energy Scavenging for Wireless Sensor Networks". In: *Norwell*, pp. 45–47.

Roundy, Shad and Yang Zhang (Feb. 28, 2005). "Toward Self-Tuning Adaptive Vibration-Based Microgenerators". In: *Smart Structures, Devices, and Systems II*. Smart Structures, Devices, and Systems II. Vol. 5649. International Society for Optics and Photonics, pp. 373–385. DOI: 10.1117/12.581887.

Rutishauser, Matthew et al. (Jan. 2011). "CARNIVORE: A Disruption-Tolerant System for Studying Wildlife". In: *EURASIP J. Wirel. Commun. Netw.* 2011, 10:1–10:14. ISSN: 1687-1472. DOI: 10.1155/2011/968046.

Sari, Ibrahim, Tuna Balkan, and Haluk Külah (2010). "An Electromagnetic Micro Power Generator for Low-Frequency Environmental Vibrations Based on the Frequency Upconversion Technique". In: *Journal of Microelectromechanical Systems* 19.1, pp. 14–27.

Schmutz, Joel A. and Gary C. White (1990). "Error in Telemetry Studies: Effects of Animal Movement on Triangulation". In: *The Journal of Wildlife Management* 54.3, pp. 506–510. ISSN: 0022-541X. DOI: 10.2307/3809666. JSTOR: 3809666.

Sera, D., R. Teodorescu, and P. Rodriguez (June 2007). "PV Panel Model Based on Datasheet Values". In: *2007 IEEE International Symposium on Industrial Electronics*. 2007 IEEE International Symposium on Industrial Electronics, pp. 2392–2396. DOI: 10.1109/ISIE.2007.4374981.

Settaluri, Krishna T., Hsinyi Lo, and Rajeev J. Ram (June 1, 2012). "Thin Thermoelectric Generator System for Body Energy Harvesting". In: *Journal of Electronic Materials* 41.6, pp. 984–988. ISSN: 1543-186X. DOI: 10.1007/s11664-011-1834-3.

Shafer, Michael W. and Eric Morgan (2014). "Energy Harvesting for Marine-Wildlife Monitoring". In: *ASME 2014 Conference on Smart Materials, Adaptive Structures and Intelligent Systems*. American Society of Mechanical Engineers, V002T07A017–V002T07A017.

Shafer, Michael W et al. (Feb. 1, 2015). "The Case for Energy Harvesting on Wildlife in Flight". In: *Smart Materials and Structures* 24.2, p. 025031. ISSN: 0964-1726, 1361-665X. DOI: 10.1088/0964-1726/24/2/025031.

Shafer, Michael William (2013). "Piezoelectric Vibrational Energy Harvesters: Designs, Limits, and Applications to Avian Bio-Logging". Ph.D. United States – New York: Cornell University. 151 pp. URL: https://search.proquest.com/docview/1466022362/abstract/C1C54BEA402C4F08PQ/1 (visited on 10/15/2018).

Snowdon, Maisie M. et al. (2018). "Feasibility of Vibration Energy Harvesting Powered Wireless Tracking of Falcons in Flight". In: *Journal of Physics: Conference Series* 1052.1, p. 012049. ISSN: 1742-6596. DOI: 10.1088/1742-6596/1052/1/012049.

Sommer, Philipp et al. (2016). "Information Bang for the Energy Buck: Towards Energy-and Mobility-Aware Tracking." In: *EWSN*, pp. 193–204.

Spreemann, D. et al. (2006). "Non-Resonant Vibration Conversion". In: *Journal of Micromechanics and Microengineering* 16.9, S169. ISSN: 0960-1317. DOI: 10.1088/0960-1317/16/9/S01.

Sravanthi Chalasani and James M. Conrad (Apr. 2008). "A Survey of Energy Harvesting Sources for Embedded Systems". In: *IEEE SoutheastCon 2008*. Southeastcon 2008. Huntsville, AL, USA: IEEE, pp. 442–447. ISBN: 978-1-4244-1883-1 978-1-4244-1884-8. DOI: 10.1109/SECON.2008.4494336.

Stark, I. (Apr. 2006). "Invited Talk: Thermal Energy Harvesting with Thermo Life". In: *International Workshop on Wearable and Implantable Body Sensor Networks (BSN'06)*. International Workshop on Wearable and Implantable Body Sensor Networks (BSN'06), pp. 19–22. DOI: 10.1109/BSN.2006.37.

Starner, T. (1996). "Human-Powered Wearable Computing". In: *IBM Systems Journal* 35.3.4, pp. 618–629. ISSN: 0018-8670. DOI: 10.1147/sj.353.0618.

Stengel, Robert F. (Oct. 16, 2012). *Optimal Control and Estimation*. Courier Corporation. 1083 pp. ISBN: 978-0-486-13481-9. Google Books: JqDDAgAAQBAJ.

Sun, Yang et al. (2011). "An Comparator Based Active Rectifier for Vibration Energy Harvesting Systems". In: *Advanced Communication Technology (ICACT), 2011 13th International Conference On*. IEEE, pp. 1404–1408.

Tan, Huiling, Alan Wilson, and John Lowe (Feb. 1, 2008). "Measurement of Stride Parameters Using a Wearable GPS and Inertia Measurement Unit". In: *Journal of biomechanics* 41, pp. 1398–406. DOI: 10.1016/j.jbiomech.2008.02.021.

Wahbah, M. et al. (Sept. 2014). "Characterization of Human Body-Based Thermal and Vibration Energy Harvesting for Wearable Devices". In: *IEEE Journal on Emerging and Selected Topics in Circuits and Systems* 4.3, pp. 354–363. ISSN: 2156-3357. DOI: 10.1109/JETCAS.2014.2337195.

Wan, Z. G., Y. K. Tan, and C. Yuen (Sept. 2011). "Review on Energy Harvesting and Energy Management for Sustainable Wireless Sensor Networks". In: *2011 IEEE 13th International Conference on Communication Technology*. 2011 IEEE 13th International Conference on Communication Technology, pp. 362–367. DOI: 10.1109/ICCT.2011.6157897.

Wang, Yiwei et al. (Jan. 22, 2015). "Movement, Resting, and Attack Behaviors of Wild Pumas Are Revealed by Tri-Axial Accelerometer Measurements". In: *Movement Ecology* 3.1, p. 2. ISSN: 2051-3933. DOI: 10.1186/s40462-015-0030-0.

Watkins, Richard (2013). "The Origins Of Self-Winding Watches 1773 - 1779". In: p. 404.

Wijesundara, Malitha et al. (Dec. 2016). “Design of a Kinetic Energy Harvester for Elephant Mounted Wireless Sensor Nodes of JumboNet”. In: *2016 IEEE Global Communications Conference (GLOBECOM)*. GLOBECOM 2016 - 2016 IEEE Global Communications Conference. Washington, DC, USA: IEEE, pp. 1–7. ISBN: 978-1-5090-1328-9. DOI: 10.1109/GLOCOM.2016.7841730.

Williams, Hannah J. et al. (Mar. 27, 2017). “Identification of Animal Movement Patterns Using Tri-Axial Magnetometry”. In: *Movement Ecology* 5.1, p. 6. ISSN: 2051-3933. DOI: 10.1186/s40462-017-0097-x.

Williams, Terrie M. et al. (Oct. 3, 2014). “Instantaneous Energetics of Puma Kills Reveal Advantage of Felid Sneak Attacks”. In: *Science* 346.6205, pp. 81–85. ISSN: 0036-8075, 1095-9203. DOI: 10.1126/science.1254885. pmid: 25278610.

Wilmers, Christopher C. et al. (2015). “The Golden Age of Bio-Logging: How Animal-Borne Sensors Are Advancing the Frontiers of Ecology”. In: *Ecology* 96.7, pp. 1741–1753.

Wilson, Alan M. et al. (2013). “Locomotion Dynamics of Hunting in Wild Cheetahs”. In: *Nature* 498.7453, p. 185.

Wu, You et al. (2014). “Multi-Source Energy Harvester for Wildlife Tracking”. In: *Active and Passive Smart Structures and Integrated Systems 2014*. Vol. 9057. International Society for Optics and Photonics, p. 905704.

Xue, T. et al. (2014). “Analysis of Upper Bound Power Output for a Wrist-Worn Rotational Energy Harvester from Real-World Measured Inputs”. In: *Journal of Physics: Conference Series*. Vol. 557. IOP Publishing, p. 012090.

Xue, Yang and Lianwen Jin (Oct. 2010). “A Naturalistic 3D Acceleration-Based Activity Dataset Amp;Amp; Benchmark Evaluations”. In: *2010 IEEE International Conference on Systems, Man and Cybernetics*. 2010 IEEE International Conference on Systems, Man and Cybernetics, pp. 4081–4085. DOI: 10.1109/ICSMC.2010.5641790.

Yang, Zhaohui, Jing Wang, and Jinwen Zhang (June 1, 2011). “A High-Performance Micro Electret Power Generator Based on Microball Bearings”. In: *Journal of Micromechanics and Microengineering* 21.6, p. 065001. ISSN: 0960-1317, 1361-6439. DOI: 10.1088/0960-1317/21/6/065001.

Yeatman, Eric M. (2008). “Energy Harvesting from Motion Using Rotating and Gyroscopic Proof Masses”. In: *Proceedings of the Institution of Mechanical Engineers, Part C: Journal of Mechanical Engineering Science* 222.1, pp. 27–36.

Ylli, K. et al. (2015). "Energy Harvesting from Human Motion: Exploiting Swing and Shock Excitations". In: *Smart Materials and Structures* 24.2, p. 025029. ISSN: 0964-1726. DOI: 10.1088/0964-1726/24/2/025029.

Yun, J. et al. (May 2011). "Design and Performance of an Optimal Inertial Power Harvester for Human-Powered Devices". In: *IEEE Transactions on Mobile Computing* 10.5, pp. 669–683. ISSN: 1536-1233. DOI: 10.1109/TMC.2010.202.

Zhang, Pei et al. (2004). "Hardware Design Experiences in ZebraNet". In: *Proceedings of the 2nd International Conference on Embedded Networked Sensor Systems - SenSys '04*. The 2nd International Conference. Baltimore, MD, USA: ACM Press, p. 227. ISBN: 978-1-58113-879-5. DOI: 10.1145/1031495.1031522.

Zipfel, Peter H. (2007). *Modeling and Simulation of Aerospace Vehicle Dynamics, Second Edition*. Reston ,VA: American Institute of Aeronautics and Astronautics. ISBN: 978-1-56347-875-8. DOI: 10.2514/4.862182.